

A dual glycoengineering system: combining synthetic biology with an Artificial Golgi Column

Nicholas J DeBono

BAdvSc Biomolecular Science, Macquarie University

A thesis presented for the degree of

Master of Research

Under the supervision of

Dr Edward S.X. Moh

and

Dr Heinrich Kroukamp



MACQUARIE
University
SYDNEY · AUSTRALIA

Department of Molecular Sciences

Macquarie University, Sydney, Australia

October 2019

Declaration

I hereby certify that the work presented in this thesis titled “A dual glycoengineering system: combining synthetic biology with an Artificial Golgi Column” has not been previously submitted for any degree, nor has it been submitted for a degree to any other university or institution other than Macquarie University, Sydney. This thesis is an original piece of research and the result of my own work except where appropriately acknowledged.

Biosafety ethics for this work has been duly obtained (Yeast 2.0: 5201401059, HEK293-FT: 5201600372)

I consent to a copy of this thesis being available in the Macquarie University Library for relevant consultation, loan and photocopying.

Nicholas J DeBono

October 2019

Acknowledgements

There are too many people to thank in this work, however I would like to do my best.

First and foremost, to my two supervisors, Ed and Heinrich. Without your help this year would not have happened, nor would I have had as fun a time as I did. Ed, thanks for putting up with my crazy ideas (and occasionally going along with them), and for our meetings approximately 10-12 times a day. I guess there really are benefits to having offices next to each other! Heinrich, thank you for putting up with my chaotic nature, and for our daily meetings over breakfast. It's pretty awesome knowing that there is someone who is always willing to help you with your next set of 384 PCR's, especially when we are hand pipetting. Your wedding was amazing and I feel very blessed for being given the privilege of attending.

To Nicki, thank you for your constant oversight, guidance and for continually pushing myself and Ed to try new things and get involved. Being able to work under your umbrella has truly made me a better scientist. After seeing your lecture on sugars back in first year, I never realised that I would be working on them all these years later!

To my group peers: Julian, Anastasia, Sayantani, Harry, Liz, Kai, John, Tej, Liisa, Nima, Kevin and Morten. Science is a collaborative effort and everyone has provided me with valuable advice and feedback multiple times throughout the year. My thesis would be nowhere near where it is without your help. You are all excellent scientists, and wonderful people! Thank you.

To my friends who helped me this year, thank you for putting up with my constantly bailing on catch up's and leaving early when I did come. I promise it was just my research! I'm looking forward to sharing the joy of having finished this project with each and every one of you. Whether it be proofreading, writing tips, gossip or just hanging out, I have truly appreciated the moments we have had together.

To my family. Mum and Dad, I know that you constantly say that you have never had to push me to do my work, but I still think that I owe my work ethic to both of you. Thanks for dragging me up proper, and for making sure that I'm your favourite son. To your other sons, James and Greg, thanks for giving me guidance, support and advice not just for this year, but for all the other years where I was growing up around you. I wouldn't be half the person I am today if I didn't have the both of you to look up to.

Lastly, to Sophia. This year could not have been possible without your acceptance, support and guidance. I'm looking forward to the many memories we will have in the future, and excited to share them all with you.

Other contributions during this candidature

Poster

“Controllable *in vitro* glycoengineering with an artificial Golgi column. (#491)”

Nicholas J DeBono¹, Chi-Hung Lin², Nicolle H Packer^{1,2}, Edward S.X. Moh¹

Presented at 18th Human Proteome Organization World Congress, Adelaide Convention Centre, Adelaide

Conferences attended

1. Australian and New Zealand cell and developmental biology meeting (ANZSCDB NSW)
June 12, Sydney University, Sydney
Attendee
2. 2nd Australasian Glycoscience Symposium, Adelaide (AGS)
September 14, UniSA, Adelaide
Attendee
3. 18th Human Proteome Organization World Congress (HUPO2019)
September 15 – September 19, Adelaide Convention Centre, Adelaide
Poster presentation

Table of Contents

| | |
|---|-----|
| Declaration..... | i |
| Acknowledgements..... | ii |
| Other contributions during this candidature..... | iii |
| 1 Abstract..... | 1 |
| 2 Introduction..... | 2 |
| 2.1 Native <i>N</i> -glycan biosynthesis and glycoengineering techniques | 3 |
| 2.1.1 <i>N</i> -glycan biosynthesis | 3 |
| 2.1.2 Importance of <i>N</i> -linked glycosylation in monoclonal antibody (mAb) function..... | 5 |
| 2.1.3 Types of glycoengineering..... | 8 |
| 2.2 Research Aims..... | 15 |
| 2.2.1 Creation of a glycoengineered <i>S. cerevisiae</i> strain producing a glycoengineered mAb for further coupling to the AGC. | 16 |
| 2.2.2 Proof of concept creation of an <i>in vitro</i> artificial Golgi column (AGC)..... | 16 |
| 2.2.3 Testing and optimisation of the AGC. | 16 |
| 3 Material and Methods | 17 |
| 3.1 Composition of growth media..... | 17 |
| 3.1.1 <i>Saccharomyces cerevisiae</i> strains used..... | 19 |
| 3.1.2 <i>S. cerevisiae</i> breeding, sporulation, and tetrad dissection..... | 19 |
| 3.1.3 Design of Trastuzumab, α -1,3-mannosyl-glycoprotein 2- β -N-acetylglucosaminyltransferase (<i>GnTI</i>) and α -1,2-mannosidase gene blocks..... | 19 |
| 3.1.4 Plasmid and Strain construction..... | 20 |
| 3.1.5 Integration of α -1,2-mannosidase into <i>S. cerevisiae</i> genome | 21 |
| 3.1.6 Insertion of <i>GnTI</i> at <i>MNN1</i> in <i>S. cerevisiae</i> using CRISPR/Cas9 | 21 |
| 3.1.7 Protein expression and purification from <i>S. cerevisiae</i> | 21 |
| 3.1.8 Recombinant galactosyltransferase production and HEK293-FT transfection..... | 21 |
| 3.1.9 Column creation for AGC..... | 22 |
| 3.1.10 3D printing a standard column..... | 22 |
| 3.1.11 Transferase purification and immobilisation | 23 |
| 3.1.12 Preparation of glycoprotein substrate for AGC experiments..... | 23 |
| 3.1.13 AGC experiment | 24 |
| 3.1.14 Leaching testing of AGC. | 25 |
| 3.1.15 SDS-PAGE and staining of proteins | 25 |
| 3.1.16 <i>N</i> -glycan release..... | 26 |
| 3.1.17 <i>N</i> -glycan analysis | 26 |
| 4 Results..... | 27 |
| 4.1 Development of an <i>in vivo</i> production system | 27 |

| | | |
|--------|---|----|
| 4.1.1 | Breeding of <i>S. cerevisiae</i> for double and triple knockout creation..... | 27 |
| 4.1.2 | Integration of α 1,2-mannosidase (<i>MNS1B</i>) gene..... | 29 |
| 4.1.3 | Trastuzumab transformation and production..... | 30 |
| 4.1.4 | Secreted protein glycomics of yeast strains..... | 32 |
| 4.1.5 | Using CRISPR/Cas9 to replace the <i>MNN1</i> ORF with <i>GnTI</i> | 33 |
| 4.2 | Development of a scalable <i>in vitro</i> glycoengineering system..... | 34 |
| 4.2.1 | Treatment of Bovine Fetuin with α 2-3,6,8 neuraminidase and β 1,4-galactosidase..... | 34 |
| 4.2.2 | Testing the leaching of glycosyltransferases from the Ni-NTA beads..... | 35 |
| 4.2.3 | Production of glycosyltransferase enzymes in HEK293-FT cells..... | 37 |
| 4.2.4 | Initial testing of the B4GalT1-AGC..... | 38 |
| 4.2.5 | Comparing AGC column format..... | 39 |
| 4.2.6 | Testing the amount of substrate in B4GalT1-AGC activity..... | 40 |
| 4.2.7 | Testing the repeatability of the B4GalT1-AGC activity..... | 40 |
| 4.2.8 | Adjusting column internal diameter parameters of the B4GalT1-AGC..... | 40 |
| 4.2.9 | Testing glycosylation of commercial Trastuzumab in the B4GalT1-AGC..... | 41 |
| 4.2.10 | Testing ST6Gal1-GFP AGC with desialylated fetuin as a substrate..... | 43 |
| 4.2.11 | B4GalT1-AGC and ST6Gal1-GFP-AGC in sequence..... | 43 |
| 5 | Discussion..... | 44 |
| 6 | Conclusion and future directions..... | 48 |
| 7 | References..... | 50 |
| 8 | Supplementary material..... | 57 |

1 Abstract

Glycoengineering aims to generate proteins with defined glycosylation. Production of glycoengineered proteins can be performed *in vivo*, with modification of gene expression of the host glycosylation enzymes pre-protein purification, or *in vitro*, using glycan modifying enzymes post-protein purification. Glycoengineering *in vivo* is scalable but requires the combinatorial generation of genetic variants. Glycoengineering *in vitro* is more controllable but increases in cost as number of enzymes involved increases.

Here a dual glycoengineering system, comprising of an *in vivo* glycoengineered *Saccharomyces cerevisiae* and an artificial Golgi column (AGC) was designed. When glycoengineered high-yield producing yeast was coupled to an *in vitro* glycosylating column, a scalable, glycan-defined glycoprotein production system was created. A target glycoprotein (Trastuzumab) is produced in *S. cerevisiae* engineered to synthesize the GlcNAcMan₅GlcNAc₂ hybrid glycan structure by disrupting genes *OCH1* and *MNN1*, while inserting α -1,2-mannosidase and *GnTI* into the genome. Subsequently, the AGC performs *in vitro* glycosylation with immobilised B4GalT1 and ST6Gal1 on-column, forming galactosylated and sialylated glycans. Physical parameters such as flowrate and substrate concentrations were partially optimised for on-column glycosylation and the reusability of the column was demonstrated. This multi-faceted approach to glycoengineering shows promise for future industrial applications with potential for large-scale glycan modification of valuable therapeutics and glycoproteins.

2 Introduction

As proteins are produced inside cells, they are subject to post translational modifications (PTM). A common PTM is protein glycosylation, wherein carbohydrate moieties, glycans, are added to proteins via the activity of glycosidases and glycosyltransferases (1). The most prominent types of protein glycosylation in human cells are *N*- and *O*-linked glycosylation. *N*-glycosylation is the covalent attachment of an oligosaccharide to the nitrogen atom of an asparagine residue within a consensus sequence of Asn-X-Serine/Threonine, where X is any amino acid but Proline (2). Where the *N*-linked glycosylation site can be predicted with high accuracy, sites of *O*-linked glycosylation are less predictable. *O*-linked glycosylation generally occurs on the oxygen atom of a serine or threonine residue, when there is a nearby proline residue (3). *N*-glycans generally have the same core structure of Man₃GlcNAc₂ (Figure 1), while *O*-glycans can have up to 8 different core structures (3).

The presence of an *N*-glycan recognition site, however, does not guarantee the addition of glycans to that site on a given peptide. Glycan addition to proteins can be dictated by steric site factors (4, 5), the protein transport through the ER, the ability of the cellular machinery to access these sites, the availability of glycan precursors or substrates, and organism specific biosynthetic pathways. Despite this unpredictability, protein glycosylation is highly significant and affects basic protein features such as folding, stability and function (2, 3). It is therefore of great interest to researchers to investigate the potential of glycosylation engineering, with the aim to improve the efficacy of current and future recombinant proteins and therapeutics. Glycoengineering is the application of engineering principles to the synthesis of glycan structures for the direct purpose of modification towards a specific target structure. This process can happen both *in vivo* and *in vitro* and draws upon techniques from various fields including molecular and synthetic biology, proteomics, genomics and, most importantly, glycomics.

Glycans have measurable effects on the glycoprotein they are connected to, affecting stability, pharmacokinetics, pharmacodynamics, bioactivity, and immunogenicity (6-8). For this reason, over the last four years, mammalian cell lines such as HEK and CHO cells have been used to produce 84% of all new biopharmaceutical products (6, 7, 9). This has achieved complex, human type *N*-glycan biosynthesis, reducing unwanted immunogenic and bioactivity effects. Of the remaining 16% of synthesised proteins made, standard non-mammalian chassis organisms such as *Escherichia coli* and *Saccharomyces cerevisiae*, which only attaches very large high mannose *N*-glycans, are used. Typically, those biopharmaceutical products produced in *E. coli* required no glycosylation (such as pro-insulin (10)); or are made in *S. cerevisiae* yeast strains that had been glycoengineered to produce more human-like glycan structures (11).

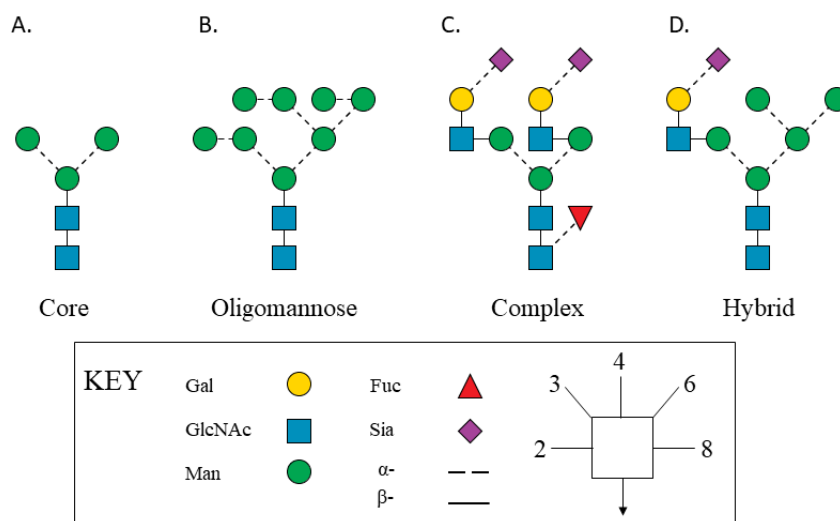


Figure 1 - Summary of N-linked glycosylation. Core N-glycan sequence (A) and three basic types of N-linked glycans are shown, with the consensus core sequence redrawn separately on the left. Oligomannose (B.), complex (C), and hybrid (D) structures are typically found on mature human glycoproteins, whereas high-mannose structures are observed on unicellular eukaryote glycoproteins, such as yeast (not shown). Symbol nomenclature based on SNFG and will be used for all subsequent figures (12). Figures adapted from (2, 3).

2.1 Native N-glycan biosynthesis and glycoengineering techniques

2.1.1 N-glycan biosynthesis

Initial stages of N-glycans synthesis are highly conserved across all eukaryotes. From initial core N-glycan ($\text{Man}_3\text{GlcNAc}_2$) synthesis, a high level of diversity is observed built on this structure. A lipid-linked oligosaccharide (LLO) precursor is assembled in the endoplasmic reticulum and transferred onto the glycoprotein. Following partial deglycosylation by glycosidases, N-glycans assist in binding to the ER-folding factor, Calnexin, which enhances protein folding. At this stage, the glycoprotein is also subject to protein quality control via the Unfolded Protein Response (UPR) pathway. If the protein has not folded properly, the N-glycan is glucosylated, which signals re-entry into the Calnexin cycle for repeated folding attempts. If the glycoprotein passes the ER quality control, then it will be further trimmed to $\text{Man}_8\text{GlcNAc}_2$ and transported to the Golgi for additional modification.

It is in the Golgi that further N-glycan modification occurs, with the differences between yeast and higher eukaryotes becoming pronounced (Figure 2). Upon entry to higher eukaryotic Golgi, the $\text{Man}_8\text{GlcNAc}_2$ is further trimmed to $\text{Man}_5\text{GlcNAc}_2$. Subsequent additions of GlcNAc and trimming of mannose results in a $\text{Man}_3\text{GlcNAc}_4$ (Figure 2). Here, depending on the glycoprotein, cell type, and available substrates, the N-glycan terminus can be further modified with the addition of GlcNAc,

GalNAc, galactose and sialic acids. These modifications happen sequentially, and result in different conformations of complex *N*-glycans (Figure 2). Glycosylation is not homogenous on individual glycoproteins, and it is seen that a heterogeneous mixture of *N*-glycans is observed in proteins produced by mammalian expression hosts (13). When designing glycoprotein therapeutics for specific targets and functions it is desirable to have a homogenous glycoforms with well-defined and predictable properties, rather than a heterogeneous mix (6).

In contrast to mammalian systems, most fungi that have been used in recombinant glycoprotein production tend to further elongate the $\text{Man}_8\text{GlcNAc}_2$ in the Golgi with additional mannose and mannosylphosphate residues. This leads to very high mannose structures as seen in Figure 2. The budding yeast *S. cerevisiae* has been shown to form hypermannosylated structures with up to 200 mannose residues (14), while *Pichia pastoris* produces structures with up to 50 mannose (14). *P. pastoris* also tends to incorporate β -1,2-linked mannose structures, which may elicit an immunogenic effect when found on therapeutics.

Due to differences in *N*-glycan biosynthesis between mammalian hosts and other eukaryotes such as yeast, it is important to consider the potential of strain engineering to produce recombinant glycoproteins with *N*-glycans that are recognised as human-similar. Where predictable properties and effector functions are sought, homogenous glycoforms on the protein are additionally required to achieve this.

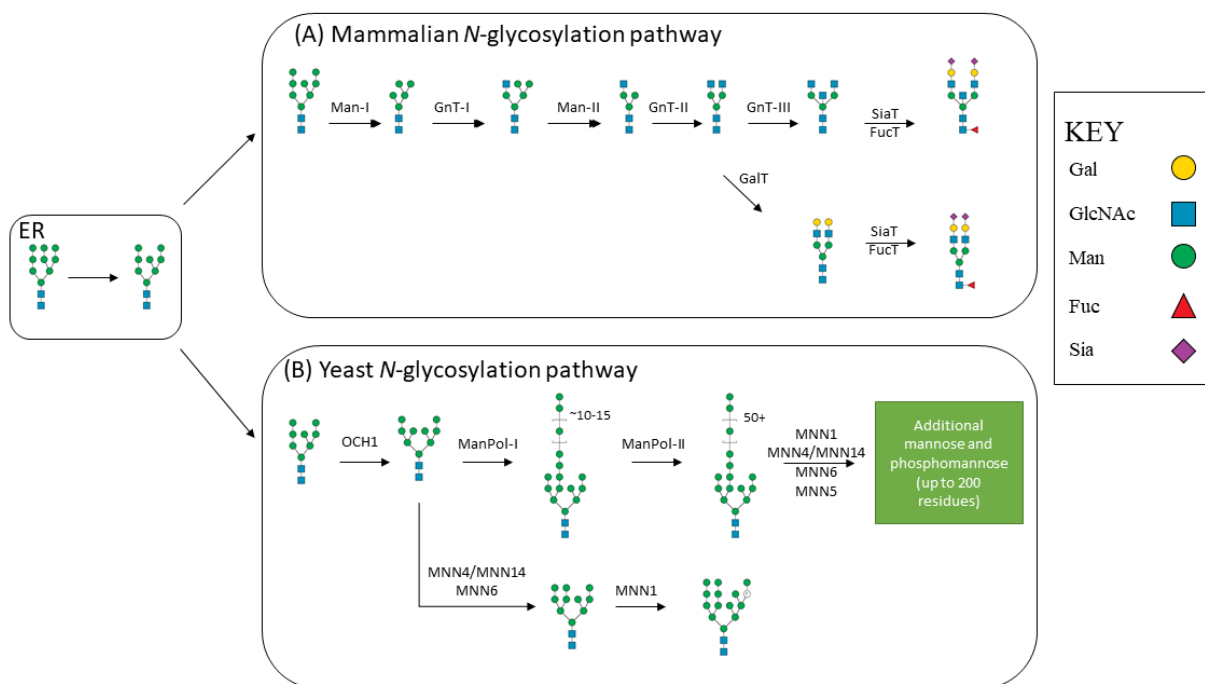


Figure 2 – Simplified glycan processing in the Golgi apparatus. (A) Mammalian cells. In the mammalian Golgi, the $\text{Man}_8\text{GlcNAc}_2$ structure is shortened to $\text{Man}_5\text{GlcNAc}_2$ through the action of

Mannosidase-I (Man-I). This is followed by the addition of a GlcNAc residue by GnT-I. Subsequently, one α -1,3 and one α -1,6-mannose residue is removed by Mannosidase-II (Man-II). The resulting GlcNAcMan₃GlcNAc₂ structure is further modified by several glycosyltransferases, resulting in a complex-type N-glycan containing galactose (by GalT), sialic acid residues (by SiaT) and/or fucose (by FucT). (B) Saccharomyces cerevisiae. Here, Man₈GlcNAc₂ N-glycans imported from the endoplasmic reticulum are modified by the α -1,6-mannosyltransferase OCH1, which adds an α -1,6-mannose to the α -1,3-mannose of the trimannosyl core. This mannose initiates the formation of hyperglycosyl-type glycans by elongating the outer chain with α -1,6-mannose residues, which is catalysed by two protein complexes, Mannose polymerase I (ManPol-I) and Mannose polymerase II (ManPol-II). The α -1,6-mannose backbone is further modified by the addition of α -1,2-mannoses, followed by mannosylphosphate residues and capping α -1,3-mannoses. Although core-type N-glycans do not often have outer chain elongation, they can be modified with α -1,2-mannose, mannosylphosphate and be capped with α -1,3-mannose. Figure adapted from (15).

2.1.2 Importance of N-linked glycosylation in monoclonal antibody (mAb) function

Monoclonal antibodies (mAbs) are currently the fastest growing and largest class of therapeutics worldwide (16). These mAbs are important therapeutic agents and have been used for the treatment of diseases, including infectious and inflammatory, as well as cancer (17). Currently, all mAbs on the market are immunoglobulin G (IgG) type and contain a fragment crystallisable (Fc) region and a highly variable (Fab) region. These mAbs are highly valuable, with Trastuzumab, an anti-HER2 IgG, holding a market value of USD \$7 052 million in 2016 (18). On the Fc region, all IgG mAbs (including Trastuzumab) contain an N-glycosylation site at Asn297. IgG is an important immunoglobulin which participates in both the innate and adaptive branches of the mammalian immune system (19). It has been previously determined that changing the Fc N-glycan structures affects effector function and biophysical properties of mAbs at a measurable level (6, 7, 20, 21). These effects have been summarised in Figure 4. Molecular simulations of the glycosylated Fc region of mAbs suggests the mechanism behind these changes is the maintenance different conformations of the Fc region of the mAbs.

2.1.2.1 Conformation changes of the Fc region.

Fc receptors can be split into two major classes, Type I and Type II. Typically, Type I receptors are a part of the immunoglobulin superfamily and include canonical Fc γ receptors (22). These Fc γ receptors are both activating (Fc γ RI, Fc γ RIIa, Fc γ RIIc, Fc γ RIIIa, and Fc γ RIIIb), and inhibiting (Fc γ RIIb). Type II receptors are from the C-type family of lectins, which mediate pathogen recognition and cell-cell interactions, activating downstream cytotoxic pathways (23, 24). Directly affected by the N-glycans located on the Asn297 of the IgG, the Fc region can be found in either

closed or open conformation (Figure 3) (22). The glycan-mediated spatial conformation of the Fc region affects the mAbs affinity towards different Fc γ receptors, affecting factors of other complement-mediated biological functions such as antibody-dependant cellular cytotoxicity (ADCC) and complement dependent cytotoxicity (CDC). The characteristics of the *N*-glycans directly impacts the conformation of the Fc region and are thereby responsible for antigen receptor specificity.

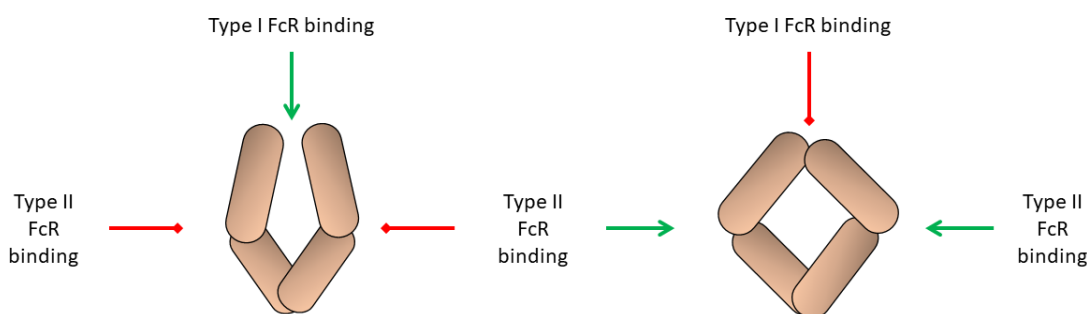


Figure 3 - Engagement of Type I and Type II FcR by the IgG Fc domain. The Fc domain alternates between the open conformation (left) and closed conformation (right), depending on the sialylation status of the Fc glycan. Upon conjugation of sialic acid, the Fc acquires a closed conformation that blocks the type I FcR-binding site and reveals a binding site for type II FcRs. Figure adapted (22).

2.1.2.2 Effect of the core fucose

A well-studied and prominent modification that can be performed on *N*-glycans attached to mAbs is the removal of the fucose on the core *N*-glycan region. Lack of core fucose leads to between a 4- and 100-fold increase of ADCC (19, 25), due to increased binding affinity between the IgG and Fc γ RIIIa and Fc γ RIIIb (26-29). The reverse of this is also true, and when core fucose is present on IgG, binding to Fc γ RIII is inhibited, reducing the inflammatory response (19, 28).

2.1.2.3 Effects of terminal galactose

It has been shown that the positive binding effects caused by the lack of core fucose were further extended when the glycans contained terminal galactoses (30). IgG's with terminal galactose on the glycans have significantly increased affinity towards C1q, the first subcomponent of the classical complement activation pathway (31), activating downstream complement dependent cell cytotoxicity (CDCC) (32, 33).

2.1.2.4 Addition of a bisecting GlcNAc

Addition of a bisecting GlcNAc to the core *N*-glycan structure on mAbs cooperates with the removal of the core fucose, providing an increase in ADCC activity. This increase is not as strong as core fucose removal alone but can still provide up to a 10-fold response in ADCC activity (34). A secondary, protecting effect of bisecting GlcNAc addition has been observed, wherein the presence

of a bisecting GlcNAc residue prevents core fucose addition and terminal sialylation of the *N*-glycan (19, 35).

2.1.2.5 Terminal sialylation

Terminal sialylation (addition of *N*-acetylneuraminic acid (Neu5Ac)), affects the inflammatory response to the IgG that it is connected to. Mechanistically, α -2,6-sialylated *N*-glycans have a stronger affinity to the same Fc γ RIIIa mentioned previously when compared with non-sialylated *N*-glycans (17). This increased affinity increases the ADCC up to threefold over an unsialylated antibody. Increased affinity from sialylation has been disputed in other literature, which instead suggests that high levels of sialylation decrease the ADCC response and reduce affinity to the Fc γ RIIIa (36). Further investigation reveals these differences in effects are due to sialylation linkage differences, α -2, 6- or α -2, 3-linked (17). α -2, 3- terminal sialylation of *N*-glycans positively affects the anti-inflammatory response of the IgG (20) and has been found to increase the half-life of many glycoproteins (36, 37). On the other hand, terminal α -2,6 sialylations enact an increased ADCC effect by increasing the conformation flexibility, forcing the Fc region into a closed conformation and enhancing affinity to bind to Type II Fc γ receptors, such as the dendritic cell-specific intercellular adhesion molecule-3-grabbing non-integrin (DC-SIGN) (22).

2.1.2.6 Increased mannose-binding lectin affinity

The presence of high-mannose and terminal GlcNAc structures on *N*-glycans of mAbs is suggested to cause increased binding affinity to mannose-binding lectin (MBL) in the body (38). Most likely this affinity is a direct result of the presence of these *N*-glycans on the cell surface of many known bacterial and virological pathogens (19), initiating the lectin complement cascade. Non-galactosylated *N*-glycans have also been shown to have an increased affinity towards MBL, but only in the absence of terminal sialylation on the other *N*-glycan arm (19, 32). It has been observed that there is a direct correlation between *N*-glycan size and structural stability of IgG, implying that those *N*-glycans which contain high-mannose structures, such as those in yeast, will often be more stable and more soluble than those structures with more truncated glycosylations (39).

2.1.2.7 Fusion Proteins

Recently it has been elucidated that *N*-glycan moieties on the variable region of fusion proteins also have a therapeutic effect, altering rates of protein clearance and availability of that molecule to cellular systems (40). Interestingly, it was found that only those *N*-glycans that contained terminal Gal or GlcNAc had increased clearance rates while introducing even one terminal sialic acid prevents this from occurring. The variable region of fusion proteins also represents a future area of interest in the glycoengineering space, especially when considering potential effects these glycans may have on PK, bioactivity, and immunogenicity.

Different moieties of *N*-glycans on the Fc region of mAbs all have varying and measurable effects which have been summarised in Figure 4. Current recombinant cell factories generally produce antibodies with heterogeneous glycan structures; many of these produce cell line specific structures such as the characteristic high mannose structures produced by yeast and the lowly abundant immunogenic Neu5Gc sialic acid additions in CHO cells. (41). With correct glycoengineering practices, the moieties produced on *N*-glycans in mAbs and other therapeutics can be controlled and targeted towards a specific purpose.

2.1.3 Types of glycoengineering

2.1.3.1 *In vivo* engineering

The requirement for correct *N*-glycosylation of therapeutics often restricts the choice of production host. Common recombinant production hosts have been listed, and their characteristics are summarised in Table 1. To enable non-mammalian hosts to be used, strain engineering is a common strategy to produce proteins with the desired glycan structures, although growth defects can also result as an undesired outcome (42-44). Thus, a balance must be found between optimum protein output and strain survival.

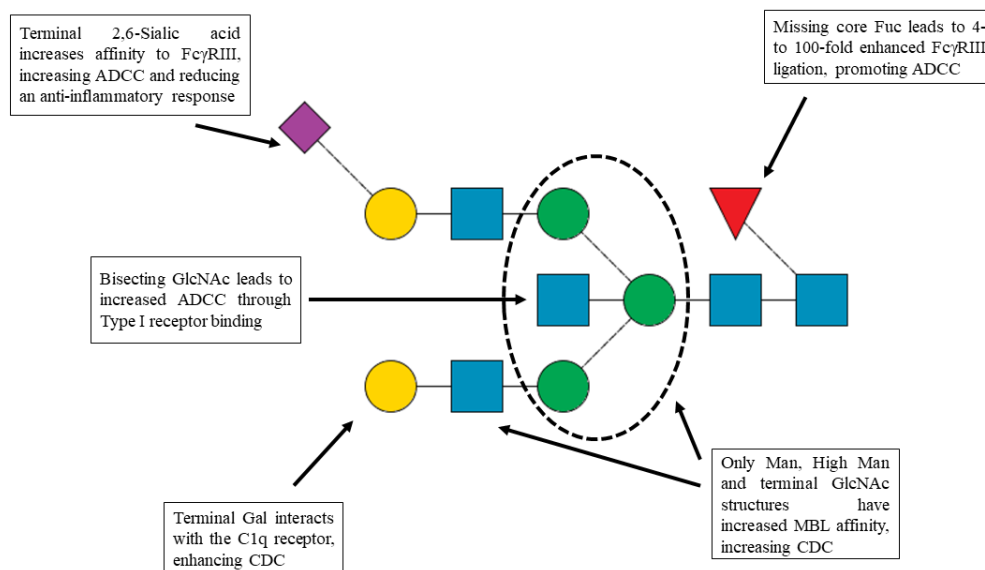


Figure 4 - A summary of altered *N*-glycosylation of IgG and its downstream effects. Figure adapted from (19)

Industrial production of therapeutics is performed most commonly in Chinese Hamster Ovary (CHO) cell lines (9, 45). Current CHO cells can produce therapeutics in quantities of up to 13 g L⁻¹, however, industry standards sit typically between 1-5 g L⁻¹ (45). This yield is far above a human recombinant cell line, HEK cells, which have been shown to produce in yields of 95-120 mg L⁻¹ (46). CHO cells

are the most extensively used cell line for production of industrial therapeutics (45) and between 1982 to 2014 have produced 35.5% of all approved biopharmaceutical proteins reported (47). Care must be taken in the production of these therapeutics due to susceptibility to infection and fragility of lines. Economically, mammalian cell lines such as CHO and HEK have a higher cost of production when compared to yeast or bacteria, such as *S. cerevisiae* or *E. coli*.

Mammalian cells have consistently been chosen over bacterial and fungal cell factories as their ability to correctly fold human proteins is unparalleled. This is a result of human proteins being inherently very similar to those proteins found in the original host organism as most of the glycosyltransferases required are already present in the host. It is important to recognise that there is a substantial difference between mammalian cell lines, particularly CHO, the standard protein secretor, and immortalised human lines such as the HEK cell line (48). When grown in identical conditions and producing an identical recombinant factor VII in CHO and HEK cells, the folding of the protein was not affected, but the resulting glycosylation was different. CHO cells usually have higher terminal sialylation, with no terminal GlcNAc residues found on the glycosylation, while HEK cells have a higher degree of structural variety, lower ratios of terminal sialylation and higher levels of terminal GlcNAcs (49).

The sialylation of CHO cells is also different when compared to human cell lines. Neu5Ac and a second form, N-glycolylneuraminic acid (Neu5Gc) are the two most common types of sialic acid attached to more than 40 different glycoforms (50). Crucially, humans have a 92- base pair deletion in the CMAH gene which encodes cytidine monophospho-Neu5Ac hydroxylase, meaning they cannot synthesise Neu5Gc (51). The presence of Neu5Gc found on glycoproteins when produced in CHO cells can elicit a human immune response and have more rapid clearance *in vivo* (51, 52). Even more crucially, prolonged treatments with Neu5Gc containing therapeutics potentially results in the accumulation of Neu5Gc in body tissue. This accumulation promotes antibody-mediated inflammation, atherosclerosis and carcinoma progression (53, 54). Thus, the production of system-specific glycan profiles is an important factor that must be considered before choosing the correct expression host.

With the advancement of recombinant protein technology, the idea that mammalian cells do not need to be exclusively used for recombinant glycoprotein production has been and will continue to be explored. Currently, simple therapeutics that do not require complex folding machinery or glycosylation are produced in simpler organisms. *E. coli*, in particular, has been used to produce many simple therapeutics such as proinsulin, interleukin, and even antibody fragments (10, 55-57). An “Expression Atlas” (58) has been created and is available online (<https://www.ebi.ac.uk/gxa/home>), containing information about gene and protein expressions in different species. This database

provides valuable information for researchers when choosing the right expression host and for seeing what has previously been produced.

Bacterial glycoengineering is also a current and ongoing field of research. A prokaryotic N-glycosylation pathway elucidated in *Campylobacter jejuni* (58) has subsequently been transferred to *E. coli* for glycosylation of production of therapeutics (58). This field may prove promising in the future but is currently limited by the lack of complex folding machinery often required to fold larger proteins (<10 kDa) required to be manufactured (59,60). An additional limitation is the tendency of glycosylated *E. coli* to incompletely glycosylate proteins, due to insufficient glycan precursor availability (60).

S. cerevisiae, like *E. coli*, has been approved for use in recombinant therapeutic production (8). *S. cerevisiae* has already been used to produce human antibodies, and molecular strain engineering has been performed on this organism to increase protein output (61-63). Glycoengineering has also taken place within *S. cerevisiae*, with the effective humanisation of this strain of yeast being well-documented (58, 64, 65) and described below. With these engineering efforts, *S. cerevisiae* IgG production has been increased 10-fold from wild type. While this yield is still quite low when compared to traditional IgG production methods (0.2 mg/L in yeast compared to a maximum of 5 g/L in CHO cells) the cost of culturing yeast is substantially lower than mammalian cells.

Table 1 - Summary of recombinant production features in different expression hosts. Table adapted from (8)

| | Yeast: <i>Pichia pastoris</i> | Yeast: <i>S. cerevisiae</i> | Insect cells (<i>SF-9</i>) | Mammalian cells (<i>CHO, HEK</i>) | Bacteria (<i>E. coli</i>) |
|---|--|--|---------------------------------------|--|--------------------------------------|
| <i>Human-like glycoproteins</i> | Yes (after strain engineering) | Yes (after strain engineering) | Partly | Yes | No |
| <i>Human protein folding</i> | Yes | Yes | Yes | Yes | Partly |
| <i>Endotoxin-free</i> | Yes | Yes | Yes | Yes | No |
| <i>Virus free</i> | Yes | Yes | Yes | No | Yes |
| <i>Development times</i> | Rapid | Rapid | Medium | Slow to middle | Rapid |
| <i>Cell growth</i> | Rapid | Rapid | Slow | Slow | Rapid |
| <i>Productivity</i> | Low to High | Low to High | Low to High | Moderate to High | High |
| <i>Potential for industrial scale-up</i> | High | High | Medium | High | High |
| <i>System cost</i> | Low | Low | Medium | High | Low |
| <i>Freedom to operate</i> | Yes | Yes | ? | Yes/No | Yes |
| <i>Approved products as of 2014</i> | 0 | 28 | 1 | 76 | 45 |

While *S. cerevisiae* has been declared as safe to use by the FDA (Generally Regarded As Safe (GRAS)), there are other species of yeasts that show great potential in the world of recombinant protein production and glycoengineering. One such species is *Pichia pastoris*. *P. pastoris* is a methylotrophic yeast, meaning it can be grown with methanol as the sole carbon source. *P. pastoris* is a worthwhile target for future recombinant engineering processes as it grows to a higher biodeensity than *S. cerevisiae* and has a stacked Golgi, more closely resembling those found in mammalian and human cell lines (68, 69). Despite this, *P. pastoris* remains a difficult organism to work with. Even though it has the capacity for increased biomass over *S. cerevisiae*, productivity may not correlate with increased biomass, and in some cases will cause a decrease in yield of product (70-72). Genetic engineering of *P. pastoris* remains a difficult task as there are developing, but a limited number of genetic tools are currently available for use. This is a consequence of the inherent instability of plasmids in *P. pastoris* during replication. By comparison, *S. cerevisiae* readily performs homologous recombination, allowing for targeted editing and accurate gene deletion. As plasmids and artificial chromosomes are essential tools in molecular biology, the extensive and highly characterised plasmid and gene library available for *S. cerevisiae* is an important factor to consider when choosing which host to express the recombinant product in. In terms of *N*-glycosylation, where *S. cerevisiae* usually produces high mannose structures of 50-150 residues, *P. pastoris* produces mannose structures of approximately 20 residues in a manner as previously shown (Figure 2). As both *N*-glycan moieties are discordant with traditional human *N*-glycans further glycoengineering needs to be performed. Here, *S. cerevisiae* has an advantage, as *P. pastoris* lacks a mannosyltransferase that confers α -1,3-linked mannosyl terminal linkages (73).

Early steps in yeast glycoengineering for both *P. pastoris* and *S. cerevisiae* involve the elimination of the *OCH1* gene, encoding α -1,6-mannosyltransferase and responsible for the initial stages in outer chain elongation (74). Once this deletion has occurred, other essential genes in the *N*-glycan biosynthesis pathway such as *MNN1* and *MNN4* are removed to ensure a homogeneous core glycan of Man₃GlcNAc₂. Following this, addition of glycosidases and glycosyltransferases such as α -1,2-mannosidase and β -1,2-*N*-acetylglucosaminyltransferase are required to generate a partially 'humanised' *N*-glycan (75, 76). Critically, it is important to ensure that the ability to add sialic acids and galactose residues is engineered into yeast strains, as this terminal glycosylation with Neu5Ac is one of the defining features of human glycosylation (77). Several strains of *P. pastoris* with truncated and/or humanised glycosylation have been produced and are commercially available (8, 69, 79-85). Strains were produced by GlycoFi, a company that has since been purchased by Merck & Co. in 2006 (83). These strains in *P. pastoris* have already been used to produce various mAbs such as Herceptin

(80). For reasons previously mentioned, strain development and research are often still performed in *S. cerevisiae* before moving to *P. pastoris*, as *P. pastoris* is more recalcitrant to genetic manipulation.

When comparing direct titre levels of human proteins produced in mammalian and non-mammalian cell lines, it is important to look at the Space-Time Yield (STY), rather than individual titre per cell. STY considers not only individual titre per cell, but also total culture time and biomass density as well. When comparing mammalian cells with other expression hosts such as *P. pastoris* or *E. coli*, the slow culture times bring CHO cells back on par with other producers. With a difference of 50 hours in *P. pastoris* to 21 days in CHO cells to produce the same amount of protein (70), protein production rate and STY is an essential factor to consider.

The advent of *in vitro* glycoengineering enables the choice of *in vivo* host to be less restrictive and the method of modification to be more modular. *In vivo* hosts can produce truncated glycoproteins and more focus can be put on the intrinsic features of the organism chosen, such as secretion factor, total protein output, and cost of growth. All potential expression hosts are now more readily available as selection is less restrictive, allowing for greater choice of production and variability. For example, testing can be performed in organisms with a high level of molecular tools such as *S. cerevisiae*, optimising the final product. Adding glycosylation steps *in vitro* post-protein production enables researchers to synthesise and identify optimal glycan structures for therapeutic proteins, depending on the function of that protein and the desire of the researcher.

2.1.3.2 *In vitro* engineering

To overcome the biological complexities of controlling glycan engineering *in vivo*, the simplest solution is to remove the most complex part – life itself. *In vitro* glycoengineering approaches utilise methods to adapt and modify glycoproteins in a cell-free environment, where multiple physical parameters can be readily controlled. Temperature, reaction mix, and substrates used are all examples of parameters that are not easily adjustable when working *in vivo*. There have been several types of *in vitro* engineering that have been performed, each with their own advantages and disadvantages.

2.1.3.2.1 Chemoenzymatic glycoengineering using mutant endoglycosidase

Perhaps the most impactful example of *in vitro* glycoengineering to date has been the creation of endoglycosidase mutants which are able to synthesise new glycans on the Fc region of mAbs with high specificity (84). Endoglycosidases such as Endo-D and Endo-S have a dual function, with the primary being hydrolysing *N*-glycans such as those found on Fc region of mAbs. Their second function is as a glycosyltransferase specific to oxazoline donor sugars (84-86). This secondary activity is strongly inhibited by the hydrolytic activity of the enzyme, so by changing key amino acid residues on the active site, Lai Xi Wang and his team have created a suite of endoglycosidase mutants only capable of transglycosylation and are not endoglycosidic (85). They achieve this by first using the unmodified

endoglycosidases to cleave existing glycans on a mAb down to a homologous truncated structure, usually fucosylated or non-fucosylated GlcNAc. Once cleaved, the mAb transglycosylated with synthetic oxazoline glycans using the mutated endoglycosidase.

This chemoenzymatic method of synthesis is very promising for production of homogenous glycoform protein therapeutics (85). However, the requirement of having a large amount of oxazoline functionalised glycans, obtained either by chemical synthesis or cleaved, purified and functionalised from other glycoproteins, makes it currently challenging for large scale production. Ideally, a modular system of glycan addition that is highly specific, cost effective, and scalable is needed to keep up with global production of mAbs and other valuable glycoproteins. One such idea is to use immobilised enzymes in a continuous flow format.

2.1.3.2.2 Free and immobilised enzymes

Broadly, different types of *in vitro* engineering can be achieved using either free or immobilised enzymes. Free enzymes have been used on multiple occasions (87-92) and have advantages in that they often represent as close to natural state as possible. Immobilised enzymes, however, are reusable, and have the potential for much higher throughput when placed in a continuous flow system. Kinetically, it is possible that immobilised enzymes are subject to a less than ideal environment as they are by definition bound to an immobile phase (93), which may impede enzyme structure and ability to interact with its target substrate. Glycosyltransferases, regarding this aspect, should be less affected as they are type II membrane proteins, naturally anchored in the Golgi membrane. Thus, immobilising these transferases on stationary phases such as resin beads mimics the Golgi environment they originate from. Furthermore, recent publications involving immobilised enzyme reactors (IMER) have shown to be promising (94-98), and the reusability of such enzymes comes with a reduced cost of production.

The majority of the protein glycosylation pathway in the human body happens in the Golgi apparatus (Figure 2, (68)). Thus, one direction to control glycosylation is to artificially recreate this Golgi, forming a synthetic, *ex vivo* system which is not reliant on living systems. This system would operate in isolation, free from other pathway interaction. Initially, this concept has been demonstrated in a microfluidic format (99), where researchers worked with heparin sulphate chains were immobilised on magnetic nanoparticles. It was this work that demonstrated the feasibility of using multi-enzyme systems to synthesise final glycan products.

A theoretical synthetic Golgi apparatus had been proposed (100), this time with a specific focus on producing the highly valuable therapeutic monoclonal antibodies. Klymenko (100) identifies glycosylation as one of the most critical quality attributes, stating that the efficacy of individual

glycoforms is unknown due to an inability to produce and test them *in vitro*. Producing many glycans from one individual precursor oligosaccharide enables the unique characteristics of each moiety to be assessed. As previously described, it is known that various terminal saccharides and removal of core fucose has a measurable and significant effect on the activity of IgG. What is unknown is the effect of addition of other saccharides in orientations that are not native to the untouched form of that antibody. There may be a receptor space that is waiting to be filled, increasing ADCC many folds, or enhancing serum half-life, that is sitting just outside the explored space.

In vitro glycosylation methods such as the artificial Golgi column described by Klymenko (100) or the microfluidic Golgi chip first made by Martin et. al (99) allow for completely synthetic structures to be made that would not be possible if created *in vivo*. By applying quality by design principles such as a repetitive build test learn cycle and mathematical modelling, steps can be taken to ensure the reduction of cost to therapeutic protein production, and an increase in the speed of this production. An important point to note is that *in vitro* glycoengineering methods such as this do not aim to build the entire *N*-glycan from scratch but build on top of an existing glycan. *N*-glycans play essential roles in folding and stability of many therapeutic molecules, and it is valuable to keep them present during the production and folding process *in vivo*. Thus, a future direction of *in vitro* glycoengineering may be as further downstream processing, additionally modifying a therapeutic before it is released as a final product.

2.2 Research Aims

As the effects of different glycosylations on mAbs have been elucidated, it has become apparent that glycoengineering is a viable avenue to increase yield and efficacy of IgG and other therapeutics. Approaches to glycoengineering have previously been undertaken both *in vivo* and *in vitro*. Yeast strains such as *P. pastoris* and *S. cerevisiae* are well-established high-secretors, proving themselves as having potential for future glycoengineering and overtaking CHO cells as the primary producer of glycoprotein therapeutics. *In vitro* IMERs show promise in downstream on-column processing, enabling high throughput glycoengineering whilst retaining expression host viability.

As *in vitro* engineering does not aim to create the *N*-glycan from scratch, it is logical to look for enzymatic reactions that start with an *in vivo* synthesised glycan with either a core or slightly more mature *N*-glycan structure. Picking a point ‘halfway’ through the process of *N*-glycan building divides the load between *in vivo* hosts and *in vitro* systems, potentially creating a glycoprotein platform with superior production economics. *In vivo* systems benefit from a reduced metabolic and carbon load as less non-native genes need to be engineered into their *N*-glycan biosynthesis pathway. Terminal galactosylation is an appropriate starting point for the development of an *in vitro* Golgi system, herein termed an artificial Golgi column (AGC). Galactose sugar residues form the precursor

monosaccharide for terminal sialic acid addition (101). As previously shown, these terminal sialic acids, particularly α -2,6 sialylation, increase Type Fc γ receptor binding and the anti-inflammatory properties of IgG through the conformational change they enforce on the Fc region of the IgG. Even without additional terminal sialylation, galactosylation on its own confers additional affinity to the CDCC pathway, increasing IgG cytotoxic properties.

The aim of this thesis is thus the proof-of-concept creation and testing of an *in vitro* artificial Golgi column for coupling to an existing *in vivo* *S. cerevisiae* host production system. Specifically:

2.2.1 Creation of a glycoengineered *S. cerevisiae* strain producing a glycoengineered mAb for further coupling to the AGC.

A basic and minimally glycoengineered *in vivo* production system for Trastuzumab was developed in *S. cerevisiae*, with the intention of eventually coupling to the *in vitro* AGC to produce a homogenous, glycoengineered Trastuzumab. After glycoengineering, *S. cerevisiae* strains were designed to produce a hybrid *N*-glycan, Man₅GlcNac₃ (Figure 5), containing one arm capable of interacting with those B4GalT1 and ST6Gal1 enzymes present in the AGC.

2.2.2 Proof of concept creation of an *in vitro* artificial Golgi column (AGC).

β -1,4-galactosyltransferase 1 (B4GalT1) and a terminal sialyltransferase, β -galactoside α -2,6-sialyltransferase 1 (ST6Gal1) are both appropriate glycosyltransferase enzymes for the AGC. These enzymes are type II transmembrane proteins, natively localised in the trans-Golgi. B4GalT1 adds galactose sugars onto the GlcNAc of a growing glycan structure using UDP-galactose. Similarly, ST6Gal1 adds a sialic acid in α 2,6 conformation to galactose residues present on *N*-glycans using CMP-N-acetylneuraminic acid. Together, these two proteins should be able to build terminal α -2,6 sialylated *N*-glycans *in vitro*, creating a human-like complex glycan (Figure 5).

2.2.3 Testing and optimisation of the AGC.

Several *in vitro* parameters are explored for optimisation using existing highly characterised glycoproteins, bovine fetuin and a commercially available anti-HER2 mAb, Trastuzumab, as experimental substrates. Fetuin *N*-glycans are optimised for use through the AGC by prior treatment with exoglycosidases, α 2-3,6,8 Neuraminidase and β -1,4-galactosidase, creating terminal GlcNAc tri-antennary *N*-glycans (A3). Trastuzumab *N*-glycans were not pre-treated with exoglycosidases prior to testing through the AGC and contained terminal fucosylated GlcNAc bi-antennary (FA2) *N*-glycan structures.

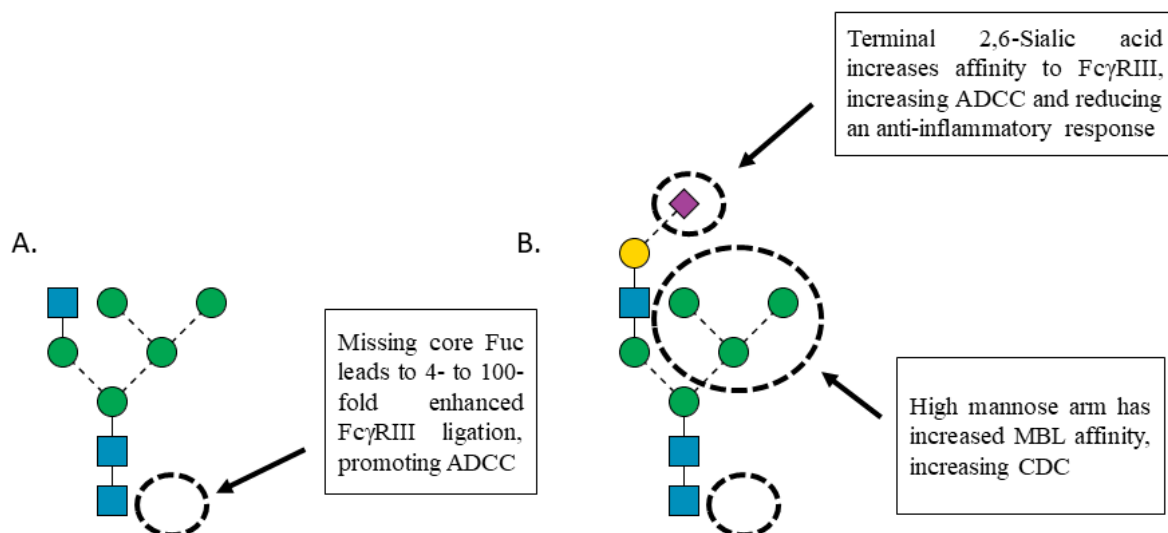


Figure 5 – Target N-glycans for in vivo production host *S. cerevisiae* (A) and AGC (B). Through minimal strain engineering, a hybrid N-glycan, *Man₅GlcNAc₃*, is produced in *S. cerevisiae* (A), compatible through the terminal GlcNAc for the *B4GalT1* glycosyltransferase enzymes present in the AGC. After treatment with the AGC, the target N-glycan is comprised of a 2,6-sialylated arm and a high mannose arm (B). These arms both induce specific effector responses for mAbs as shown in figure.

3 Material and Methods

Unless otherwise stated, all materials were obtained from either ThermoFisher Scientific Australia or Sigma Aldrich (Sydney, Australia). Deionised water was sourced from a Millipore Academic MilliQ system. Peptide N-glycosidase F (PNGase F) was obtained from Promega (Sydney, Australia).

Restriction endonucleases PacI, AscI and NotI, and the Monarch Plasmid Miniprep Kit were all sourced from New England Biolabs. Purified monoclonal Trastuzumab antibodies produced in CHO cells was purchased from Focus Bioscience (St Lucia, QLD, Australia).

3.1 Composition of growth media

Table 2 - Composition of various growth media used throughout this work.

| Type of Media | Composition | Organism |
|---|---|----------------------|
| YPD* (Yeast extract peptone dextrose) | 1% yeast extract, 2% peptone, 2% glucose | <i>S. cerevisiae</i> |
| YPD ^{geneticin*} | 1% yeast extract, 2% peptone, 2% glucose, geneticin (200 mg/L) | <i>S. cerevisiae</i> |

| | | |
|---|---|----------------------|
| (Yeast extract peptone dextrose with geneticin) | | |
| SC^{-uracil*} (double-strength synthetic complete without uracil) | 2% glucose, 1% ammonium sulphate, 2% succinate, 0.34% Yeast Nitrogen Base without amino acids, yeast synthetic drop-out medium supplements without uracil (manufacturer's guidelines), pH 6.0 (adjusted with NaOH) | <i>S. cerevisiae</i> |
| SC^{-histidine*} (double-strength synthetic complete without uracil) | 2% glucose, 1% ammonium sulphate, 2% succinate, 0.34% Yeast Nitrogen Base without amino acids, yeast synthetic drop-out medium supplements without histidine (manufacturer's guidelines), pH 6.0 (adjusted with NaOH) | <i>S. cerevisiae</i> |
| Galactose SC^{-uracil} (double-strength synthetic complete without uracil) | 2% galactose, 1% ammonium sulphate, 2% succinate, 0.34% Yeast Nitrogen Base without amino acids, yeast synthetic drop-out medium supplements without uracil (manufacturer's guidelines), pH 6.0 (adjusted with NaOH) | <i>S. cerevisiae</i> |
| Min^{41*} (Minimal S. cerevisiae BY4741 media) | 0.06% Yeast Nitrogen Base without amino acids, 0.01% leucine, 0.01% methionine, 0.01% uracil, 0.05% histidine | <i>S. cerevisiae</i> |
| LB^{ampicillin*} (Luria Broth) | 1% tryptone, 1% NaCl, 0.5% yeast extract, ampicillin (100 µg/mL) | <i>E. coli</i> |
| DMEM^{FBS} (Dulbecco's Modified Eagle's Medium with foetal bovine serum) | 90% high-glucose Dulbecco's Modified Eagle's Medium (DMEM), 10% Foetal Bovine serum (FBS), penicillin/streptomycin (100 U/ml) | HEK293-FT |
| PEI transfection medium | Freestyle 293 medium, plasmid DNA (3 µg/mL), polyethyleneimine (PEI) (9 µg/mL) | HEK293-FT |
| HEK293-FT expression medium | Freestyle 293 medium, valproic acid (2.2 mM final concentration, penicillin/streptomycin (100 U/ml), | HEK293-FT |

* - Where solid media was needed this media was made with 2% agar and poured into plates.

3.1.1 *Saccharomyces cerevisiae* strains used

Laboratory strains of *S. cerevisiae* BY4741 (102) and knockout library BY4741 - $\Delta och1$ obtained from Euroscarf haploid yeast ORF deletion library (103). Strains were spotted onto YPD^{geneticin} plates and grown at 30 °C with shaking (200 RPM) (Infors HT Multitron Pro). BY4741 strains containing $\Delta mnn1$, $\Delta MNN4$ and $\Delta MNN14$ deletions were also obtained from the same library and re-cultured under the same conditions.

3.1.2 *S. cerevisiae* breeding, sporulation, and tetrad dissection

Yeast strains of compatible mating types (mat A and α) were bred together to introduce multiple knockouts in the same strain. Pre-cultures were grown in 1 mL YPD^{geneticin} overnight at 30 °C with shaking, then 100 μ L aliquots of each strain were combined in 1 mL of YPD^{geneticin} and grown at 30 °C overnight with shaking to allow mating. 100 μ L aliquots were then spotted onto Min⁴¹ plates, which were then incubated at room temperature in the dark for 4 days to allow sporulation.

Before tetrad dissection, diploid strains were confirmed by observing the presence of asci via brightfield microscopy. A scraping of cells was then taken from plate, resuspended in 50 μ L of deionised water with 2 μ L of zymolase suspension added. Suspension was then incubated at room temperature for 5 min then diluted ten-fold. 8 μ L of the dilution was streaked in a line on a YPD^{geneticin} plate. Cell suspension was then checked for asci's using a tetrad dissecting microscope (Singer MSM 400) and spores were separated and seeded as individual spots on the plate. Plates were grown at 30 °C for 36 hours. Strains were screened for gene knockouts by first lysing colonies with a LiOAc-SDS solution and subsequently precipitating DNA with ethanol as described by Lööke et. al (104). Gotaq DNA polymerase (Promega) and primers specific to gene loci of interest on extracted DNA in a PCR, according to manufacturer protocol (Sup. Table 1). PCR products were visualised by agarose (1% w/v) gel electrophoresis.

3.1.3 Design of Trastuzumab, α -1,3-mannosyl-glycoprotein 2- β -N-acetylglucosaminyltransferase (*GnTI*) and α -1,2-mannosidase gene blocks

3.1.3.1 Trastuzumab

A gene block encoding the anti-HER2 immunoglobulin G, Trastuzumab, for production in *S. cerevisiae* was designed. The amino acid sequence for Trastuzumab was obtained from DrugBank.ca (<https://www.drugbank.ca/drugs/DB00072>), reverse-translated and codon optimised for expression in *S. cerevisiae* using Geneious Prime v11.0.3+7. Both heavy chain and light chain of this antibody were placed under the bi-directional *GAL1/10* native inducible galactose promoter. A secretion sequence containing native *OST1* secretion signal and pre-pro α -factor secretion sequence was designed based on published work by Fitzgerald et. al (44) and introduced to the N-terminus of both

chains of Trastuzumab. Native terminator sequences from *S. cerevisiae* genes *PGK1* and *ENO1* were used to terminate the heavy and light chain respectively. Each section of the gene block had a specific 8 bp restriction endonuclease site to facilitate removal and replacement of sections within the gene block if necessary. Gene block was ordered on a pUC57 cloning vector from Genscript USA, then transferred to yeast vector pRS416 (Sup. Figure 1) for transformation into *S. cerevisiae*, described below.

3.1.3.2 *GnTI*

For design of *GnTI*, the amino acid sequence of human α -1,3-mannosyl-glycoprotein 2- β -N-acetylglucosaminyltransferase was obtained from Uniprot (Accession number: Q9XGM8), reverse translated and codon optimised using Geneious Prime. A Golgi localisation tag from the *S. cerevisiae* protein KRE2 was placed at the N-terminus of the *GnTI* ORF. Finally, native constitutive promoter and terminator sequences from *S. cerevisiae* genes *PGK1* and *CYC1* respectively were added to the gene block in their appropriate positions.

3.1.3.3 α -1,2-mannosidase

For design of α -1,2-mannosidase, the amino acid sequence was obtained from *Aspergillus phoenicis* and reverse-translated and codon optimised for *S. cerevisiae* in the same manner as previously stated. Like *GnTI*, the native promoter and terminator sequence from *PGK1* and *CYC1* respectively were added to the gene block in their appropriate positions. Gene block was ordered on a pUC57 cloning vector from Genscript USA and transferred to a yeast vector (Sup. Figure 2) for transformation into *S. cerevisiae*, described below.

3.1.4 Plasmid and Strain construction

Standard protocols were used for expression vector preparation (105). For Trastuzumab gene block, a double restriction digest of NotI and AscI in Cutsmart buffer at 37 °C for 1 hour was performed. The yeast vector, pRS416 was digested in the same way. Zymoclean Gel DNA Recovery kit (Zymo Research) was used according to the manufacturer's instructions to purify restriction enzyme digested DNA from agarose gels. T4 DNA ligase was used to ligate Trastuzumab and pRS416 fragments overnight according to manufacturer's specifications. The newly ligated plasmid was then transformed using Mix & Go! chemically competent BL21 Turbo *E. coli*. Cells were incubated with 4-5 μ g of plasmid on ice for 10 minutes, then plated onto LB^{ampicillin} and grown at 37 °C. Plasmid was then purified using the Monarch plasmid miniprep kit, and yeast transformations were performed by the LiOAc-DMSO protocol (106), then plated on to agar SC^{-uracil} plates.

An integrative plasmid specific to the *FLO8* ORF was obtained from Dr. H Kroukamp (unpublished work). The α -1,2-mannosidase gene block and this plasmid were digested and ligated together as described above, using AscI and PacI as restriction endonucleases.

3.1.5 Integration of α -1,2-mannosidase into *S. cerevisiae* genome

Integration of α -1,2-mannosidase into the *FLO8* ORF was performed using transformation protocols previously described. After transformation, strains were grown in 1 mL pre cultures of Galactose *SC^{uracil}* with hygromycin B (200 mg/mL) for 6 hours to ensure integration. After this preculture step, strains were plated on *SC^{uracil}* plates and grown at 30 °C for 30 hours. PCR with primers specific to the internal sequence of α -1,2-mannosidase were used to confirm the presence of a successful integration.

3.1.6 Insertion of *GnTI* at *MNN1* in *S. cerevisiae* using CRISPR/Cas9

Target sequence for CRISPR/Cas9 in *MNN1* was selected by searching within the ORF for a suitable PAM sequence. Sequence location was 845-864 bp from start of ORF (5'-AGTTTCGATCATAAAACTGGT-3'). This sequence was inserted into a guide RNA expression vector (Sup. Figure 4) using flanking region primers (Sup. Table 1) and subsequent assembly in yeast.

GnTI was amplified from pUC57 vector with primers containing flanking regions homologous to *MNN1* ORF. CRISPR/Cas9 cleavage of *MNN1* ORF allows for high frequency of insertion of the α -1,2-mannosidase at the *MNN1* locus through homologous recombination. Co-transformation of pMMN1-guide vector containing Cas9 and linear amplified *MNN1* flanked α -1,2-mannosidase expression cassette was performed using the LiOAc-DMSO protocol. Putative transformed yeast colonies were selected on *SC^{Histidine}* plates and verified with PCR using primers specific to the *MNN1* flanked α -1,2-mannosidase regions (Sup. Table 1).

3.1.7 Protein expression and purification from *S. cerevisiae*.

250 mL of *S. cerevisiae* strains containing Trastuzumab plasmid were grown in Galactose *SC^{uracil}* in 2 L baffled culture flasks over 30 hours at 30 °C with shaking (120 RPM). Yeast cells were pelleted by centrifugation and supernatant was loaded onto a 1 mL Hi-Trap Protein G column (GE Healthcare) according to manufacturer's specifications. Bound antibodies were then eluted using 6 CV of glycine-HCl (pH 2.7), and 0.5 mL fractions collected in Eppendorf tubes containing 200 μ L of 1 M Tris-HCl (pH 9.0) to neutralise the pH. Fractions were concentrated to approximately 10x concentration using 10 kDa molecular weight cut-off (MWCO) centrifugal filters and 11 μ L of concentrate was used for SDS-PAGE gel analysis, performed as mentioned below.

3.1.8 Recombinant galactosyltransferase production and HEK293-FT transfection

Mammalian expression vectors containing genes coding for human β -1,4-galactosyltransferase (B4GalT1) were purchased from DNASU plasmid repository (107), on pGen1 and pGen2 vectors. α -2,6-sialyltransferase (ST6Gal1) on a pGen2 vector was kindly provided by Dr. Chi-Hung Lin (Institute for Glycomics, Griffith University). Both vectors contain a coding region for an *N*-terminus

8xHis/Strep purification tag, and pGen2 contains a GFP fusion linker between the purification tag and expressed protein.

Vector transformation was achieved by transforming *E. coli* as previously stated. Successful transformants were taken and grown in 2 L LB^{ampicillin} for 24 hours. Plasmid was isolated from lysed *E. coli* using the Promega midiprep kit as per manufacturers specifications. Plasmid was analysed for purity using a Nanodrop 2000 spectrophotometer and kept at -20 °C until needed.

Adherent HEK293-FT cells were obtained and grown at 37°C, 5% CO₂ in high-glucose Dulbecco's Modified Eagle's Medium (DMEM) with 10% Foetal Bovine serum (FBS). At 60-70% confluency, cells were transfected using a modified polyethylenimine (PEI) (Polysciences) transfection protocol initially described by Au – Subedi et. al with previously purified glycosyltransferase vectors (108). In short, cells were washed twice with phosphate buffered saline (PBS), before introducing 15 mL of pre-warmed PEI transfection medium containing required plasmid DNA. After a 4-hour incubation, 25 mL of additional HEK293-FT expression medium was added, and cells were left to incubate for 5 days. Culture supernatant containing the secreted enzymes was collected and centrifuged at 1000 rpm for 10 minutes to remove dead cells and other debris. Supernatant was collected in 50 mL falcon tubes and samples were stored at -30 °C until required for use.

3.1.9 Column creation for AGC

To connect the AGC to a continuous flow system an industry standard fitting was needed on either end. Existing millimetre scale columns are only available at a minimum of 10 mm internal diameter (I.D.). To reduce costs and scale of prototypic experiments two 1 mL plastic syringes (Hapool Medical Technology), which have a male Luer slip fitting connection at the base, were connected. By cutting two syringes at the 300 µL mark then heating with a Bunsen, the hot plastic ends can be fused together (Figure 6). This created a column with a male Luer slip fitting on either end, enabling connection to a continuous flow system. The internal diameter (ID) of the syringe was measured at 4.2 mm, with an internal volume of ~600 µL. Subsequent column creations revealed problems with this method, often resulting in columns that were not straight, internal defects at the joint and leaks.

3.1.10 3D printing a standard column

To overcome column inconsistency, 3D printed columns of a similar internal diameter and shape were used. A pre-drawn male Luer slip fitting was downloaded from GrabCad (www.grabcad.com), an online engineering community. User Daniel Clark designed this part, which was imported into Creo Parametric v5.0.0.0 student edition (PTC Inc.) and connected to both ends of a cylinder with parameters outlined below (Table 3).

The 3D CAD file was then exported as a high resolution .STL file and imported into Preform v3.0.2 (Formlabs Inc.). Here, the auto support tool was used to correctly orient and support 3D structures whilst they were printing. After supports were added, file was sent to a Formlabs Form 2 printer for 3D printing using clear methylacrylic acid ester (Formlabs Clear Resin v4).

Table 3 - Defined parameters for 3D printed columns

| Parameter | 4 mm I.D. | 3 mm I.D. |
|---|------------------|------------------|
| Internal diameter | 4 mm | 3mm |
| External diameter | 10 mm | 10 mm |
| Wall thickness | 6 mm | 7 mm |
| Length | 47 mm | 84 mm |
| Internal volume | 600 μ L | 600 μ L |
| Approximate length of packed resin | 15.67 mm | 28.00 mm |

Columns were removed from the printer after printing and washed with two cycles of 100% ethanol, 100% isopropyl alcohol, and water to remove any uncured resin that may remain in the column. Curing of printed resin was performed using a 405 nm UV light box for 30 minutes and left overnight at 70 °C. To increase clarity of columns, they were coated in clear nail varnish (Nail experts) post-curing.

3.1.11 Transferase purification and immobilisation

Freshly charged nickel-nitrilotriacetic acid (Ni-NTA) 0.4 μ m agarose resin beads used for enzyme immobilisation and purification were equilibrated in HEPES-HCl pH 7.4 containing 150 mM NaCl after stripping nickel ions with EDTA and charging with nickel acetate. Approximately 1 mL of this equilibrated resin was added to thawed culture media from transfected HEK293 cells containing secreted 8xHis-Strep tagged transferases, spiked with 10 mM imidazole and 150 mM of NaCl to reduce non-specific binding. Culture was rocked for an hour at 4 °C, then protein bound resin was collected by sedimentation and packed into 3D printed column, plugged with cotton wool.

3.1.12 Preparation of glycoprotein substrate for AGC experiments

In preparation for the AGC experiment, 7.5 mg of bovine fetuin was treated with either α 2-3,6,8 Neuraminidase to remove terminal sialic acids, or with α 2-3,6,8 Neuraminidase (NEB) and β -1,4-galactosidase (Prozyme) to remove both terminal sialic acids and galactose residues. Treatment was performed in a 2 mL Eppendorf tube, with 1500 μ L of 50 mM ammonium acetate pH 5.5. 50 units of α 2-3,6,8 Neuraminidase and 2 milliunits of β -1,4-galactosidase were added to each reaction, which

was incubated overnight at 37 °C. Exoglycosidase activity was confirmed via SDS-PAGE gel and LC-PGC-ESI-CID-MS/MS analysis as described below.

3.1.13 AGC experiment

A running buffer of HEPES-HCl pH 7.4 was prepared for all AGC column experiments. Injections for each experiment contained final concentrations of 10 mM MnCl₂, 150 mM NaCl, 100 nmols of appropriate donor sugars (either UDP-galactose or CMP-N-acetylneuraminic acid) and substrate glycoprotein. Both running buffer and reaction mixture were prewarmed to 37 °C before use.

Packed columns were connected to the loading pump of a Dionex Ultimate 3000 HPLC and kept in the column oven at 37 °C. Appropriately treated fetuin or commercial Trastuzumab was injected with corresponding reaction mixture into their AGC's containing the applicable transferase via a switching valve, which was then used to redirect samples to the column with a flow rate of 200 µL/min (Figure 6). Glycoprotein samples and other substrates in the reaction mix were in contact with the enzymes in the column for one minute.

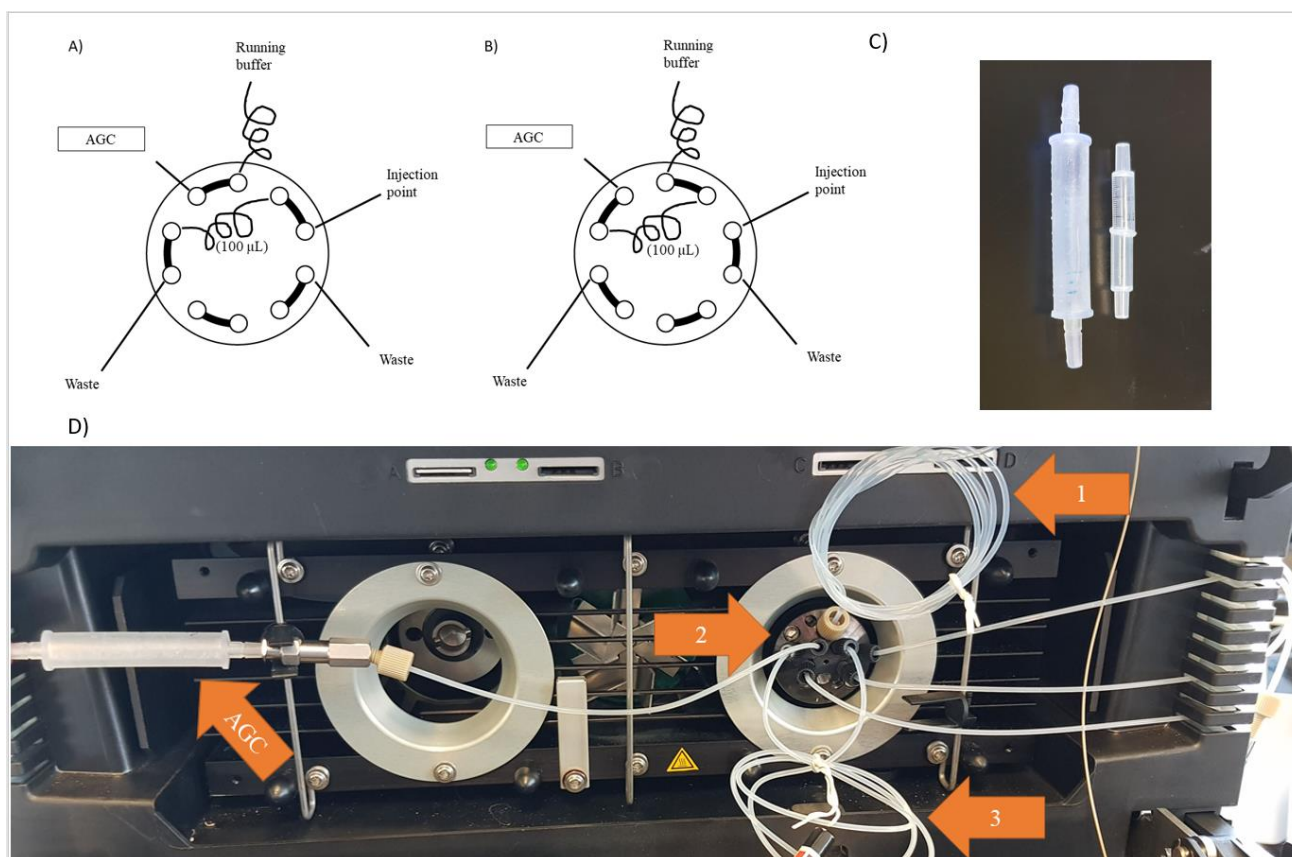


Figure 6 - Switching valve schematic for AGC experiments with columns. Sample is first injected into the 100 µL sample loop via the injection port [A], and valves are then switched, redirecting the buffer flow through the sample loop, and pushing sample reaction mixture towards the AGC [B]. Buffer is temperature equilibrated through use of an equilibration loop that sits within the column

oven with the AGC. [C] [Left] 4mm I.D. 3D printed column. Column has been 3D printed using a Form 2 printer to be compatible with an LC system and have an internal volume of 600 μ L. [Right] syringe LC compatible column. Two 1 mL syringes have been cut in half and the ends melted together using a Bunsen. [D] An image of the AGC set up is included, clearly showing the temperature equilibration loop (1), switching valve (2), and 100 μ L sample loop (3).

One mL of flow-through was collected containing eluted reaction mix with glycoprotein substrate in Eppendorf tubes containing 50 μ L of 10 mM of K_2PO_4 pH 8.0 to precipitate the $MnCl_2$ by forming $Mn_3(PO_4)_2$, stopping any transferase reaction, if present. Samples were then stored at 4 $^{\circ}C$.

3.1.14 Leaching testing of AGC.

To test possible leaching of His-tagged glycoproteins bound to Ni-NTA resin beads, 6xHis tagged superfolder-Green Fluorescent Protein (sfGFP) (109) was produced in *E. coli* grown in 500 mL of $LB^{ampicillin}$ at 37 $^{\circ}C$ overnight with shaking. Cells were then sonicated for 10 minutes and centrifuged at 15 000 g for 45 minutes. Supernatant containing 6xHis-sfGFP was collected and stored at -21 $^{\circ}C$.

Two hundred μ L of freshly charged Ni-NTA beads were added into a 3D printed column as described previously. This column was then connected to a Bio-Rad NGC chromatography system with a running buffer of HEPES-HCl pH 7.4. Washing with 50 mM of L-Histidine was performed to prevent non-specific binding of proteins, and 5 mL of supernatant injected into the system so that the 6xHis-sfGFP could bind to the Ni-NTA beads present. Once binding was complete, the bound beads were washed with increasing concentrations of $MnCl_2$ (1 mM, 10 mM, and 0.5 M), testing if these concentrations affected the binding of the protein. All steps were performed at a flow rate of 100 μ L/min. After testing, sfGFP was eluted with 0.5 M imidazole. Elution of proteins and sfGFP fluorescence was checked with an inbuilt UV photometer, checking for wavelengths of 280 nm (protein) and 485 nm (sfGFP excitation).

3.1.15 SDS-PAGE and staining of proteins

NuPAGE 4-12 % bisacrylamide-Tris (Bis-Tris) mini protein gels (12 wells) were used for multiple experiments. 3-(*N*-morpholino)-propanesulfonic acid (MOPS) running buffer at a constant voltage of 150 V with a running time of 80 min was used to separate various proteins and glycoproteins. Between 10-30 μ g of protein treated with 12.5 mM DTT and NuPAGE 4x sample loading buffer was heated to 95 $^{\circ}C$ for 15 minutes, then loaded into the gel. After gel electrophoresis, gels were fixed for half an hour in 40 % (v/v) ethanol, 10 % (v/v) acetic acid and stained with Coomassie blue on a shaker overnight at room temperature. Once staining was complete, gels were de-stained in 10 % (v/v) methanol, imaged using a Bio-Rad Gel Doc imager and analysed using Image Lab v6.01 (Bio-Rad).

3.1.16 *N*-glycan release

N-glycan release and subsequent analysis were performed as described by Jensen et. al. (110). Briefly, glycoproteins were immobilised and released as described in Jensen et al (110), with 3 technical replicates for each sample. Approximately 10 µg of glycoproteins were vacuum blotted onto ethanol activated PVDF membrane. Membrane was dried at room temperature, then blots were visualised with 0.1% direct blue stain. Glycoprotein spots were cut out with a holepunch, transferred to a 96-well low-bind plate, blocked with 1% Polyvinylpyrrolidone (PVP), and *N*-glycans were released with PNGase F overnight at 37 °C. After release, *N*-glycan containing supernatant was collected into separate Eppendorf tubes and glycosylamines were removed from reducing end of glycans by incubation with 100 mM ammonium acetate pH 5.5 for 1 hour. Samples then dried in a speed vac at room temperature (John Morris Scientific).

Following drying, samples were reduced with 1 M sodium borohydride in 50 mM potassium hydroxide at 50 °C for 3 hrs. This reaction was neutralised with 2 µL glacial acetic acid and desalted using AG 50W X8 strong cation exchange resin (200-400 mesh, 30 µL bed volume) (Bio-Rad) packed into C18 staged tips via centrifugation. Flow through containing the glycans were dried in a speed vac then reconstituted with 100% (v/v) HPLC-MS grade methanol to remove residual borate by forming volatile methylborate. Once residual borate was no longer visible in dried samples, an additional carbon clean-up step was performed. Porous Graphitised Carbon (PGC) was packed onto C18 stage tips, then washed using 90 % (v/v) acetonitrile (ACN) with 0.05 % (v/v) aqueous trifluoroacetic acid (TFA) and equilibrated with deionised water. Glycan samples were loaded through the columns twice, washed with deionised water before final elution using two rounds of 25 µL 40 % (v/v) ACN with 0.05 % (v/v) TFA. Purified *N*-glycans were then dried in the speed vac and stored at -20 °C until LC-MS/MS analysis, where they were rehydrated in HPLC-grade water.

3.1.17 *N*-glycan analysis

Purified *N*-glycans were separated and detected by LC-PGC-ESI-CID-MS/MS performed on an LTQ Velos Pro ion trap mass spectrometer (Thermo Scientific, Australia) coupled to a Dionex Ultimate 3000 HPLC (Thermo Scientific, Australia). The *N*-glycan containing samples were loaded on a PGC HPLC capillary column (Hypercarb KAPPA, 5µm particle size, 250Å pore size, 0.18 x 100 mm, Thermo Scientific) and separated using a linear gradient of 2.6 - 64 % (v/v), 70% ACN/10 mM ammonium bicarbonate over 86mins at a 3µL/min with Post-column Make-up Flow of 100% ACN at 4 µL/min (111). The acquisition range is 500-2000 m/z, a resolution of m/z 0.25 full width half maximum and a source voltage of +2.7 kV. Detection was performed in negative ionization polarity mode with data-independent acquisition.

.RAW files of mass spectrometric data were then imported into Skyline v19.1.0.193 (112), and base peak integration performed on target *N*-glycans for relative quantitation. Values were converted into proportional abundances between parent and child *N*-glycans, and graphs generated using GraphPad Prism 8.0.1. (113). Annotation of glycans was performed using Oxford nomenclature, where A denotes the number of GlcNAcylated antenna, G and S describe the number of galactose residues and sialic acids respectively, and F describes a core fucose.

4 Results

Producing pharmaceutical proteins with human-similar glycosylation at economically viable scale and cost, the dualistic approach of producing high levels of glycoproteins with a 'core'-glycan structure in yeast (*in vivo*), and subsequently modifying these glycans with a continuous flow system and immobilized enzymes (*in vitro*) in an artificial Golgi column (AGC) was evaluated. Multiple parameters such as co-factor concentration, substrate amount and internal column diameter were initially tested in this proof of concept work for future research. Furthermore, two glycosyltransferases (B4GalT1 and ST6Gal1-GFP), two glycoprotein substrates (fetuin and Trastuzumab) and two AGC chambers in sequence were tested. An increase in additionally glycosylated *N*-glycan structures was consistently found, providing guidance on future research. During the development of the AGC, *S. cerevisiae* strain development was undertaken to create a high STY strain capable of producing a model antibody (Trastuzumab) with appropriate *N*-glycan moieties on its Fc region.

4.1 Development of an *in vivo* production system

The approach used here for production of defined glycoforms on recombinant proteins requires coupling of the *in vitro* AGC with an *in vivo* production system. This production host would ideally produce the glycoprotein of interest in high STY, with a homogenous *N*-glycan glycoprofile. An example of combining *in vivo* and *in vitro* glycoengineering has already been demonstrated (80). That approach resulted in a homogeneously glycoengineered mAb, Herceptin, that was produced using *P. pastoris* coupled with the Endo S chemoenzymatic glycan synthesis method mentioned previously. The *P. pastoris* had been glycoengineered to produce a majority hybrid *N*-glycan, a strategy that was adopted in this work. Here, multiple techniques were applied to create a glycoengineered *S. cerevisiae* strain producing hybrid *N*-glycans, Man₅GlcNAc₃. To do this, insertion of a Golgi-localised GlcNAc transferase was incorporated into the design of this strain, an enzyme not found in the yeast biosynthetic pathway.

4.1.1 Breeding of *S. cerevisiae* for double and triple knockout creation

Wild type strains of *S. cerevisiae* naturally produce extended mannosylphosphorylated chain *N*-glycans, with some chains up to 150 residues long (15). Unlike in *P. pastoris*, introducing a defect at

the *OCHI* (α -1,6-mannosyltransferase) ORF does not completely shorten this hypermannose *N*-glycan. Rather, it only reduces it to primarily $\text{Man}_8\text{GlcNAc}_2$ structures, with ~10% structures having a $\text{Man}_5\text{GlcNAc}_2$ glycoform. The redundancy present in the *S. cerevisiae* *N*-glycan biosynthesis pathway continues to produce these hypermannose structures, so a quadruple knockout strain was designed containing $\Delta OCHI$, $\Delta MNN1$ (α -1,3-mannosyltransferase), *MNN4* (positive regulator of the mannosylphosphate transferase *MNN6*) and $\Delta MNN14$ (putative analogue of *MNN4*) deletions, following recommendations from several papers (114, 115).

The first three genes to be knocked out in this strain were *OCHI*, *MNN4* and *MNN14*. Single deletions already existed in the Euroscarf haploid yeast ORF deletion library and in pre-existing haploid lab strains. Thus, strains of complementary mating types were bred together, with the intention to re-cross these new double knockouts with existing single deletion strains. Assisting in this process is the distinguishable phenotype of $\Delta OCHI$. At 30 hours growth, strains containing $\Delta OCHI$ are visibly smaller and rounder than their non-knockout counterparts (Figure 7). Using tetrad dissection, the Mendelian law defining random assortment of alleles applies, and if a strain within an ascii of four haploids does not exhibit growth on selective media, then one of the other three haploids should have successfully crossed and contain both gene knockouts. As the deletion library used the same gene to replace each ORF, each deletion in a double knockout needed to be confirmed individually via PCR of just outside the target ORF. A PCR product length of ~1500 bp corresponds with the geneticin resistance marker, while product lengths greater than 2500 bp indicate presence of the original gene (Figure 7). While single knockouts were confirmed for all strains from the ORF deletion library, no double knockouts could be confirmed, either due to PCR primer non-specific binding or unsuccessful crossing.

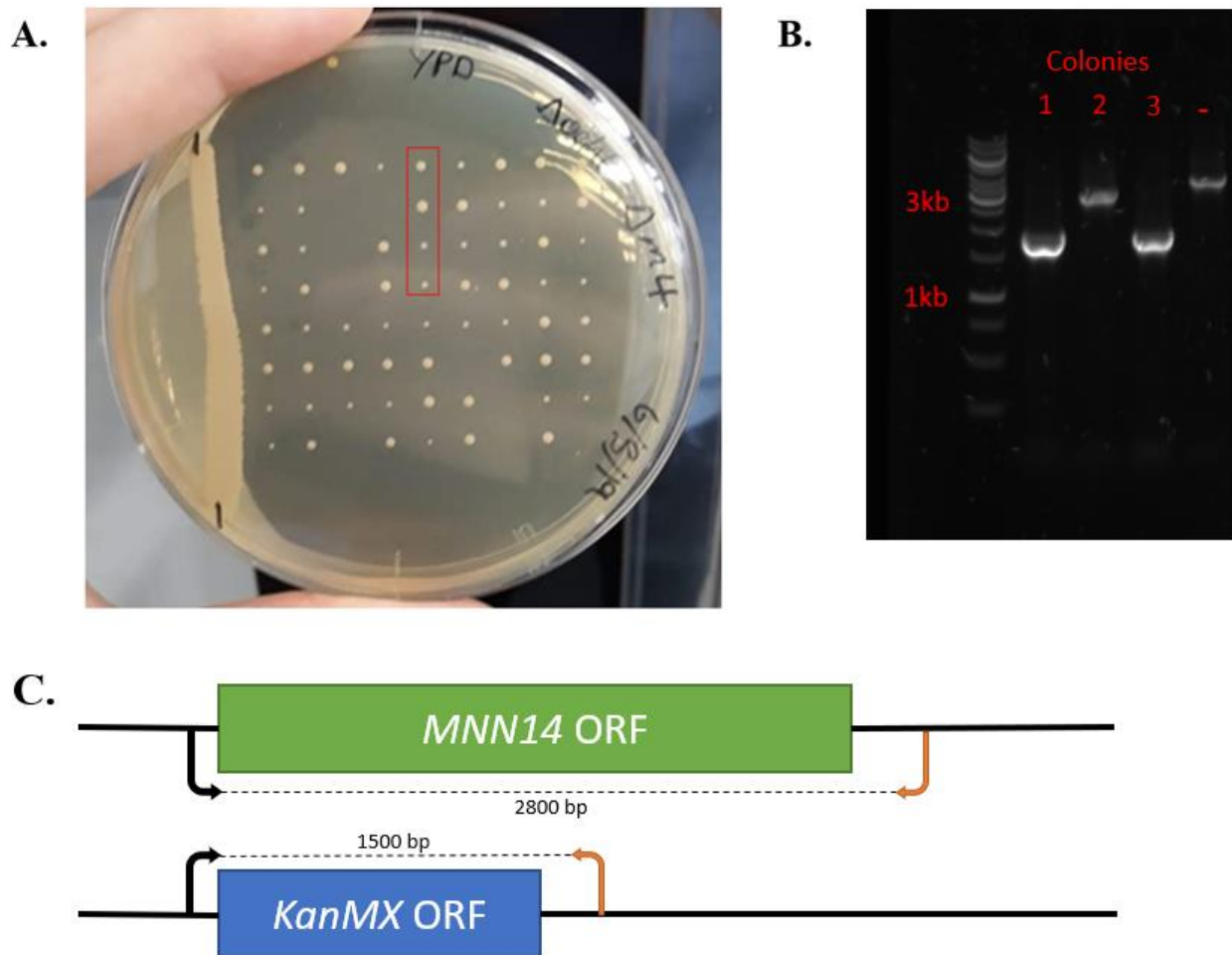


Figure 7 – [A] A typical plate representative of a tetrad dissection experiment. Colonies highlighted in the red box are single spores, all separated from the same asci. Simple Mendelian inheritance of the $\Delta och1$ was confirmed by PCR, with an observed 1:1 segregation of the *OCH1* deletion. The slow growth of the F1 segregants was exclusively linked to *OCH1* deletion. [B] A representative example of a confirmation PCR for the *MNN14* ORF. Strains that show replacement of the *MNN14* ORF with a kanamycin resistance marker show an amplification length of 1500 bp (Colonies 1 and 3), whilst strains showing no replacement have their native ORF of length 2800 bp (Colony 2). [C] Graphical representation of *MNN14* ORF replacement with kanamycin resistance marker (*KanMX*). Here, the native *MNN14* ORF has been replaced with *KanMX*, a gene conferring kanamycin resistance. As the gene is shorter, a PCR amplification of ~1500 bp is observed, rather than the native amplification length of ~2800 bp.

4.1.2 Integration of α 1,2-mannosidase (*MNS1B*) gene

Taking the BY4741 $\Delta och1$ strain, the gene block encoding α -1,2-mannosidase (*MNS1B*) was inserted into the *FLO8* ORF locus of the genome using an integrative plasmid developed in house by Kroukamp et. al (unpublished work) (Sup. Figure 2). *MNS1B*, operating under a native constitutive promoter (*PGKp*) was expected to affect further trimming of high mannose *N*-glycans, reducing

Man₈GlcNAc₂ *N*-glycans produced in $\Delta och1$ strains to Man₅GlcNAc₂ hybrid *N*-glycan structures (69). Results from Figure 8 confirm the presence of the *MNS1B* gene in a strain of BY4741 $\Delta och1$ *S. cerevisiae*. This result was confirmed using internal primers specific to this non-native gene (Sup Table 1).

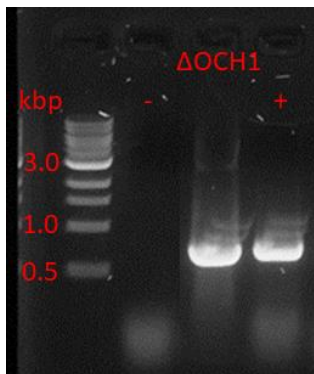


Figure 8 – Confirmation gel showing presence of α 1,2-mannosidase gene in the genome of a strain of BY4741 $\Delta och1$. Gene has been integrated into the *FLO8* ORF using homologous recombination. A successful amplification will produce a PCR product of length 730 bp. PCR primers specific to α 1,2-mannosidase were used, meaning amplification will only occur after successful integration of this gene.

4.1.3 Trastuzumab transformation and production

To produce an *in vivo* produced relevant glycoprotein substrate, the mAb Trastuzumab expression cassette was transformed into the isogenic strain BY4741, BY4741 $\Delta och1$ strains. Strains were grown in SC^{-uracil} and Galactose SC^{-uracil}. To examine the secretome of strains induced and not induced for Trastuzumab production, an SDS-PAGE was run on 250 μ L of concentrated secreted media (Figure 9). Significant differences can be seen between strains grown in glucose (uninduced) when compared to those grown in galactose (induced) media. Generally, an increase in amount of protein in the gels can be observed in those galactose strains for both BY4741 and BY4741 $\Delta och1$ through the presence of bands that are noticeably thicker and darker. This implies that the galactose promoter present on the transformed plasmid is active. Of additional importance to note is the reduced level of smearing of bands observed between the BY4741 and BY4741 $\Delta och1$ strains. As the BY4741 $\Delta och1$ strain has glycans of reduced length, they should appear as sharper and thinner bands on an SDS-PAGE. Expected bands for Trastuzumab production (25 kDa for the light chain, 50 kDa for the heavy chain and 150 kDa for the unreduced dimer cannot be directly observed in this gel, indicating a low concentration of produced Trastuzumab, if any was produced at all. Proteomic analysis of observed bands is possible to confirm the presence of Trastuzumab.

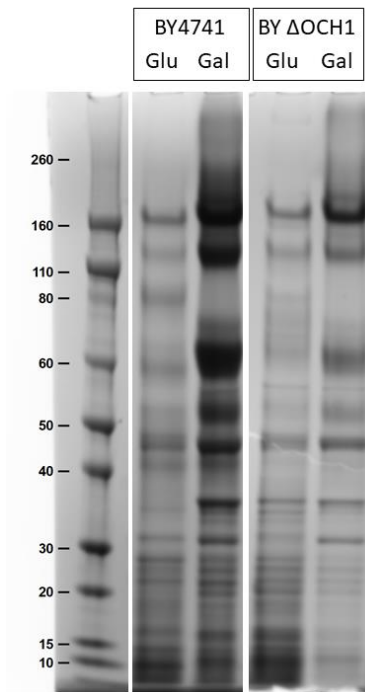


Figure 9 - SDS-PAGE gel of BY4741 and BY4741 Δ och1 secretome in glucose or galactose supplemented *SC-uracil*. Concentration of proteins in secretome are observed as being higher, due to the overall band darkness increase. A band thickening at ~45kDa may be suggestive of a heavy chain of Trastuzumab appearing under inducible conditions.

In this work to a Protein G Fc affinity column was used on 300 mL of clarified secretion media from a BY4741 Δ och1 strain containing the Trastuzumab gene cassette to confirm the production of any secreted Trastuzumab fragments. Elution from this column was performed and a 280 nm excitation was observed as bound proteins eluted from the column (Figure 10). Fractions were then collected, and concentrated samples were analysed via SDS-PAGE. Fractions 1-5 show steadily decreasing amounts of what could be the putative heavy chain of Trastuzumab eluting at ~45-48 kDa (Figure 10). Fractions 7-9 show a heavy band at ~35 kDa, indicative of the Protein G proteins bound to the resin packing of the column (Figure 10). No bands were observed at 60 kDa. This infers disintegration of the column and Protein G loss, preventing further purification or testing of any secreted yeast media at this stage.

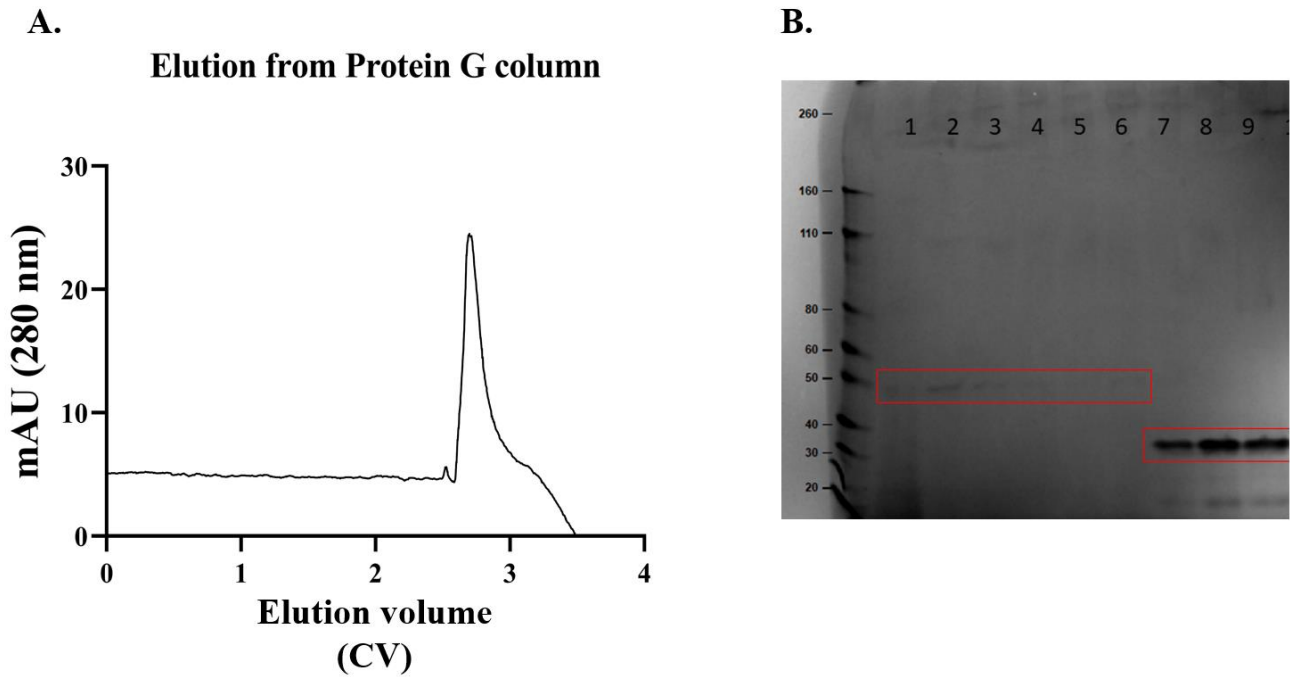


Figure 10 – [A] Trastuzumab specific binding and elution from 300 mL of BY4741 $\Delta och1$ secretion media grown in Galactose SC^{-uracil} for 30 hours. Protein G is highly specific to the heavy chain of IgG and elutes under acidic conditions of pH 2.7. Here, a sharp peak in absorbance at 280 nm is indicative of protein being eluted. [B] Elution fractions from Protein G column. Fractions are 0.4 CV in volume. Fractions 1-6 show protein bands corresponding with the expected size of the Trastuzumab heavy chain eluting at ~45-48 kDa. Fractions 7-9 feature a heavy band at 32 kDa, the correct M_r for Protein G indicating possible loss of Protein G from the column resin.

4.1.4 Secreted protein glycomics of yeast strains

To further determine the effect of performing *in vivo* glycoengineering, the yeast *N*-glycan secretome from the produced strains was analysed via LC-PGC-ESI-CID-MS/MS, and relative abundances of mannose glycans were calculated using Skyline software (Figure 11). By growing all strains in Galactose SC^{-uracil} with a Trastuzumab cassette present, higher protein output was ensured. The expected shift from predominantly Man₉GlcNAc₂ in the isogenic BY4741 strain to shorter glycan structures including Man₅GlcNAc₂ can be seen from the BY4741 $\Delta och1$ strain. When *MNS1B* was knocked into the *FLO8* ORF in the BY4741 $\Delta och1$ strain, an odd effect is observed where the lowest number of mannose structures appears to be Man₇. This is contradictory to published literature, where existing Man₈GlcNAc₂ structures present in $\Delta och1$ strains are expected to be further trimmed to hybrid Man₅GlcNAc₂ *N*-glycans (76).

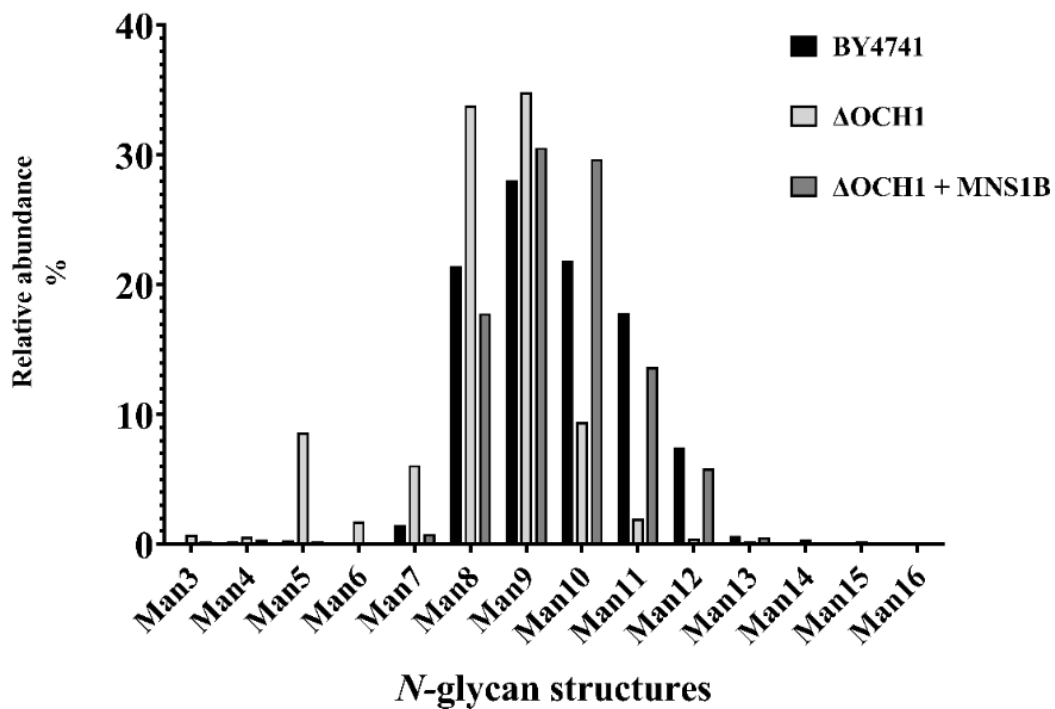


Figure 11 - A mannose glycoform profile of BY4741, BY4741 $\Delta och1$ and BY4741 $\Delta och1$ + MNS1B. BY4741 and $\Delta och1$ strains show typical high mannose glycoforms, with $\Delta och1$ strain displaying a number of Man₅GlcNAc₂ residues. The introduction of the MNS1B gene appears to have recovered the BY4741 phenotype, instead of further truncating Man₈GlcNAc₂ present in $\Delta och1$ to the hybrid Man₅GlcNAc₂ as reported in literature (76).

4.1.5 Using CRISPR/Cas9 to replace the *MNN1* ORF with *GnTI*

As the desired results were thus not obtained through breeding and whilst these additional deletions would have been desirable in creating a scalable *S. cerevisiae* host, a CRISPR/Cas9 approach was attempted to delete these genes. The use of CRISPR/Cas9 is rapidly becoming a staple in the molecular biologist's toolbox. By creating breaks in the DNA at targeted PAM sequences in the genome, homologous recombination and gene replacement can be forced by providing relatively large amounts of donor DNA with regions of homology upstream and downstream of the break. Here, a CRISPR/Cas9 plasmid developed in house by Kroukamp et. al (unpublished work) was used to replace the *MNN1* ORF with the previously designed synthetic *GnTI*. *GnTI* translates for a GlcNAc transferase (116), which will facilitate the transfer of GlcNAc structures to terminal mannose residues on *N*-glycan structures. The resulting hybrid *N*-glycan (Man₅GlcNAc) is currently a suitable starting point for the developed B4GalT1-AGC. Initially successful integration of *GnTI* cassette into the *MNN1* ORF was confirmed with PCR, using primers specific to the flanking regions of this ORF (Sup. Table 2 **Error! Reference source not found.**). To reconfirm the presence of this cassette, strains were tested using internal primers specific to *GnTI*. There was no primer amplification in any

strains, including the positive control. Because of this a primer redesign would be required in future work to confirm the presence of this cassette.

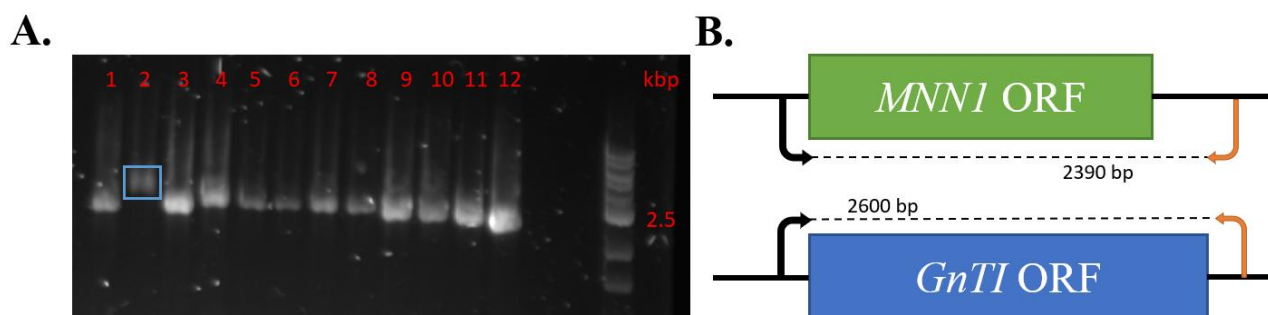


Figure 12 – Confirmation gel showing amplified PCR product of MNN1 ORF for GnTI post CRISPR/Cas9 integration. Each lane denotes a separate *S. cerevisiae* colony tested. PCR product in lanes 1 and 3-12 show the native MNN1 ORF, an unsuccessful integration with PCR product amplification length of 2390 bp. PCR product in lane 2 (blue box) exhibits a potential successful integration of GnTI, with PCR product amplification length of 2600 bp. (B) Graphical replacement of the MNN1 ORF (2390 bp) with the GnTI cassette (2600 bp).

4.2 Development of a scalable *in vitro* glycoengineering system

An AGC was designed and built for the purpose of performing specific *N*-glycan addition onto existing core *N*-glycan structures. Several different parameters were tested, and some level of improvement was made from original tests. Using treated fetuin for initial tests and then Trastuzumab as a model antibody, the intention was to develop a time efficient and scalable model for taking homogenous glycosylation towards industrial levels of production.

4.2.1 Treatment of Bovine Fetuin with α 2-3,6,8 neuraminidase and β 1,4-galactosidase

To test the AGC containing immobilised B4GalT1 and/or ST6Gal1, fetuin was chosen as the candidate substrate glycoprotein. Bovine fetuin has 3 *N*-glycans that are highly exposed and accessible for glycosyltransferases, indicated by its attached highly sialylated and tri-antennary glycans (4). For fetuin to be a suitable substrate for an AGC with immobilised B4GalT1 and ST6Gal1 glycosyltransferases, it was treated with α 2-3,6,8 neuraminidase and β -1,4-galactosidase to remove both terminal sialic acid residues and terminal galactose residues and provide a suitable substrate for these transferases. Exoglycosidase activity was verified by SDS-PAGE (Figure 13), indicated by the migration difference of the fetuin protein band relative to the control fetuin. To confirm this, control fetuin, fetuin treated with both α 2-3,6,8 Neuraminidase (Fet -S), and fetuin treated with α 2-3,6,8 Neuraminidase and β -1,4-galactosidase (Fet -S -G) were prepared for their use as substrates for the AGC. The released *N*-glycans were analysed via negative mode LC-PGC-ESI-CID-MS/MS to confirm their activity (Figure 13). Here, a clear change in *N*-glycan compositions can be seen, moving from predominantly A3G3S3 structures in untreated fetuin to A3G3 structures in Fet -S, to A3G0

structures in Fet -S -G samples. Bi-antennary structures are observable in all three traces but appear in low abundance (20 % total abundance). For this reason, analysis of glycosylation outcomes by the AGC was based on the most abundant tri-antennary glycans.

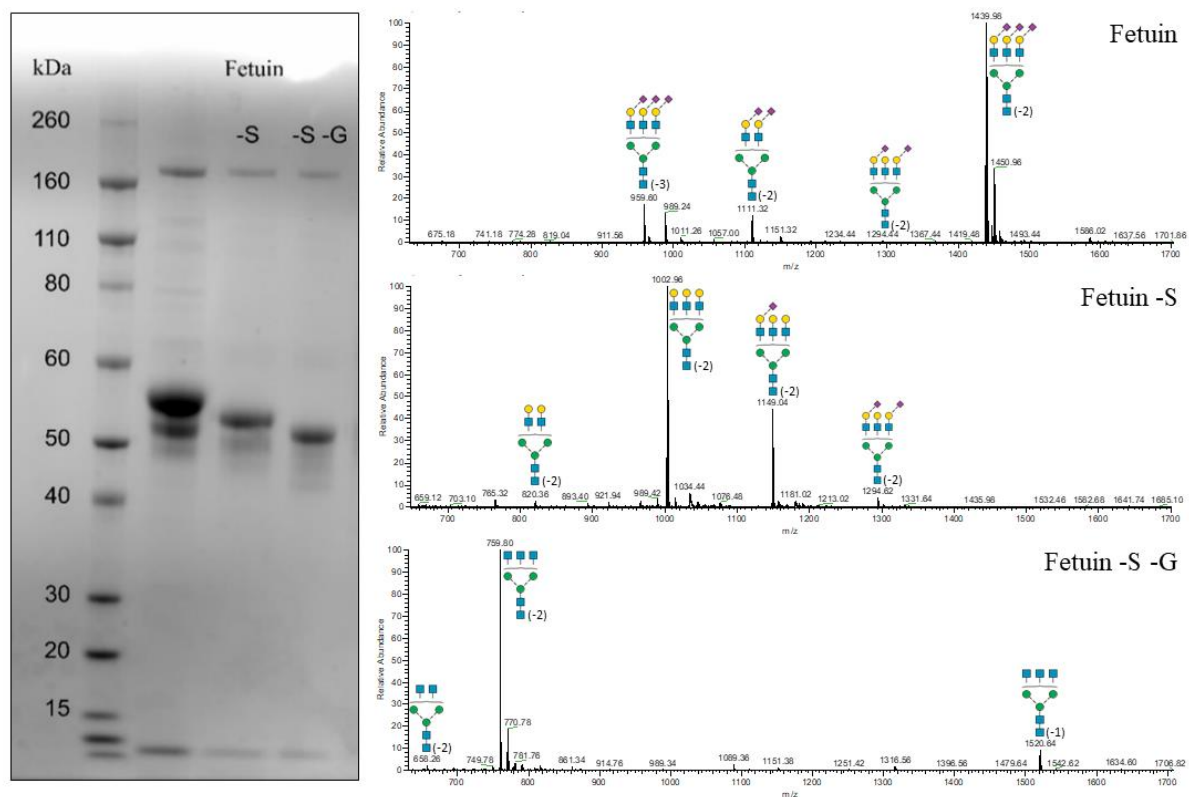


Figure 13 – [Left] SDS-PAGE of de-sialylated-de-galactosylated fetuin. Differences in migration between native fetuin, de-sialylated fetuin (Fet -S) and de-sialylated-de-galactosylated fetuin (Fet -S -G). This glycan trimming was also confirmed by released glycan mass spectrum analysis. [Right] Averaged mass spectrum of released glycans. Here the loss of terminal sialic acids and galactose residues after treatment with α -2-3,6,8 Neuraminidase and β -1,4-galactosidase is observed. Numbers in brackets next to the initial GlcNAc residue denote the charge state of the residue. Relative abundance of tri-antennary structures is significantly higher than bi-antennary structures in all samples of fetuin analysed.

4.2.2 Testing the leaching of glycosyltransferases from the Ni-NTA beads

For enzymes to be effectively immobilised, the conjugation between the glycosyltransferase and solid phase must be stable, able to remain bound through experimental conditions. Before any AGC experiments were run, the capacity of the Histidine-tags of the immobilised glycosyltransferases to remain bound to the Ni-NTA resin during experimentation was tested. If the immobilised enzymes eluted under general experimental conditions, then they are no longer reusable. Of the reagents in the experimental mix, $MnCl_2$ was most likely to affect binding capacity due to competitive binding between the Mn^{2+} ions and Ni^{2+} ions on the resin beads. To test this, a 3D printed column containing

blank Ni-NTA beads was first equilibrated, then had 6xHis tagged sfGFP from lysed *E. coli* passed through it. sfGFP was used as its production was quicker and provided a measurable cue (485 nm excitation) that could be used to directly observe bound protein leaching. Once sfGFP had bound, leaching of the column under experimental conditions for the AGC (1 mM and 10 mM MnCl₂), and then under high concentrations (0.5 M MnCl₂) was tested (Figure 14). 10 mM MnCl₂ appears before sfGFP loading as column was previously loaded with sfGFP, then re-loaded after 10 mM MnCl₂ testing.

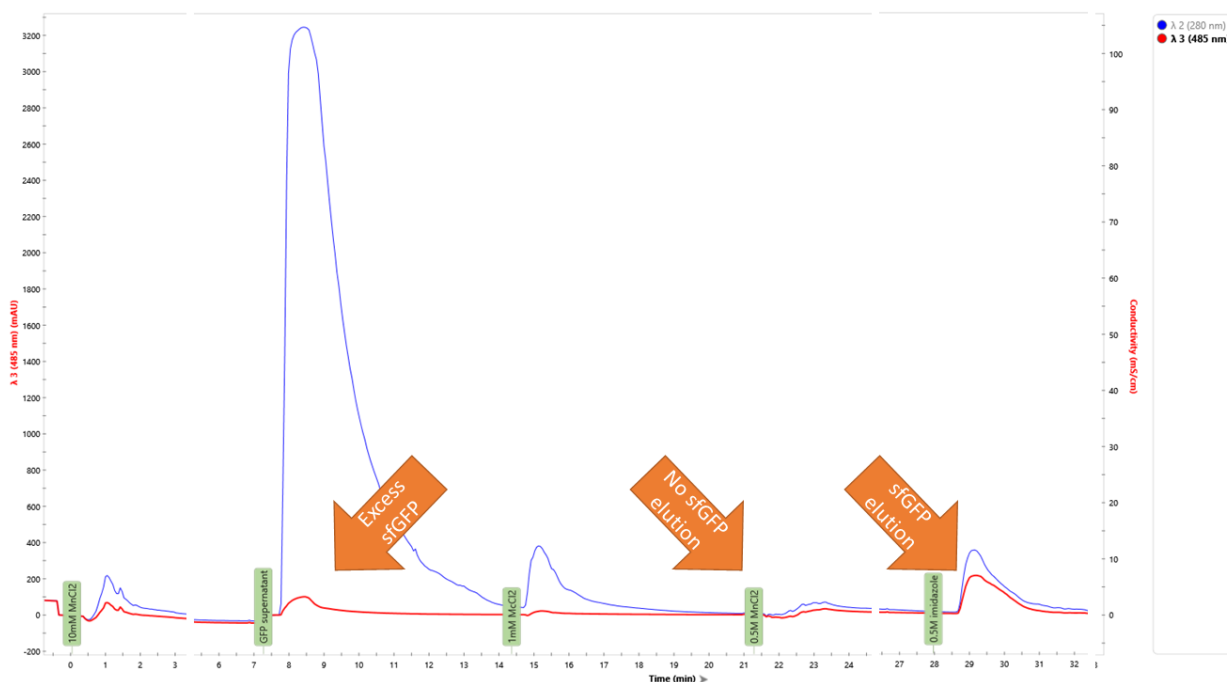


Figure 14 – Partial chromatographic trace of 280 nm (blue, protein) and 485 nm (red, sfGFP) excitation of 6xHis-tagged sfGFP bound to Ni-NTA resin in a 3D printed column. At MnCl₂ concentrations of 1, 10 and 500 mM, there is no substantial elution of sfGFP from the column, indicating the 6xHis tag binds effectively to Ni-NTA resin. When injecting 500 mM imidazole a clear elution of sfGFP is seen by an increase in 485 nm excitation. When sfGFP supernatant is injected a peak in 485 nm is observed, indicating excess sfGFP eluting from the fully bound column.

Even in extreme concentrations of MnCl₂ (0.5 M) there is little to no elution of sfGFP from the Ni-NTA resin beads. SfGFP was still visually visible on the column, and bound proteins were eluted with 0.5 M imidazole. The resultant peak in 485 nm wavelength corresponds with 6xHis-tagged sfGFP that was bound to the Ni-NTA beads eluting. This confirms that the Histidine tag conjugation is sufficient to effectively bind glycosyltransferase enzymes to the solid Ni-NTA resin used in the AGC.

4.2.3 Production of glycosyltransferase enzymes in HEK293-FT cells

HEK293-FT cells were transiently transfected with B4GalT1 (with and without GFP fusion domain) or ST6Gal1-GFP. Those vectors containing a GFP fusion domain were used so that dishes containing GFP linked enzymes provided visual cues for a positive transfection (Figure 15). A 150ul aliquot of secreted media was concentrated by evaporation and resolved on an SDS-PAGE gel to confirm the production of B4GalT1, B4GalT1-GFP and ST6Gal1-GFP. A dark band is observed at ~65-70 kDa for lanes containing B4GalT1-GFP or ST6Gal1-GFP after 5 days secretion. While the protein bands from the lanes containing the aliquots of B4GalT1 transfected HEK293-FT cells were unascertainable, as the SDS-PAGE gel melted while running (Figure 15), successful transient transfection from all other transfection plates suggests that the B4GalT1 transfected cells was also expressing the enzyme. This was subsequently confirmed with the *in vitro* galactosylation experiment via the artificial Golgi column (Figure 16).

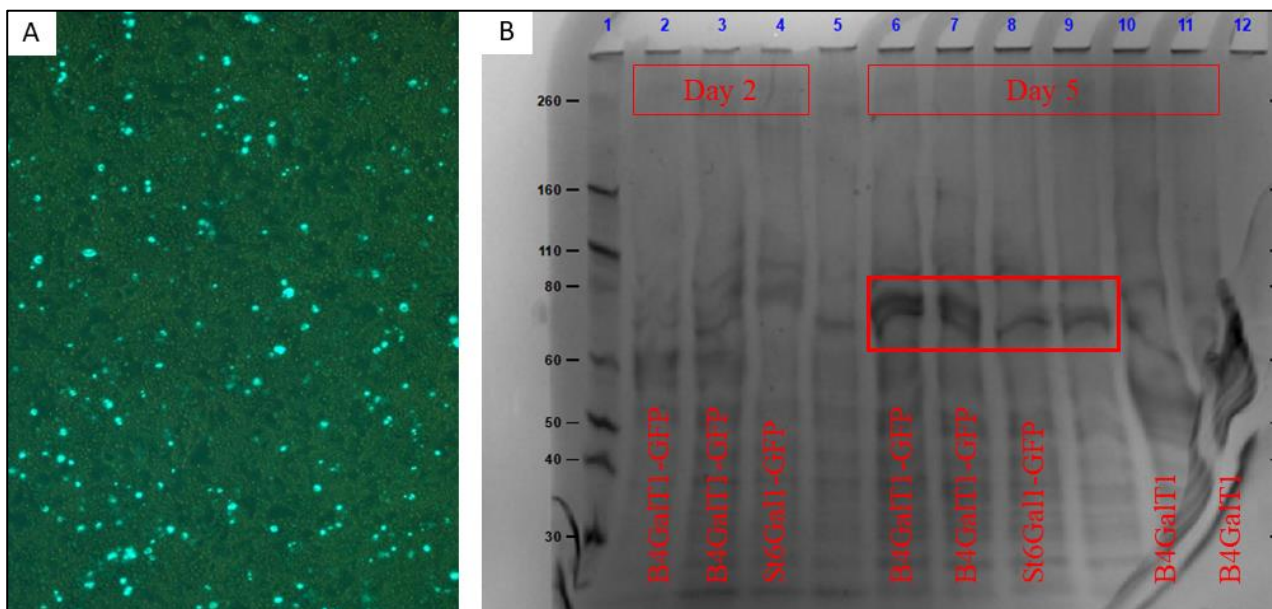


Figure 15 – Transient transfection of HEK293-FT cells. [A] A 40x microscopy image with 485 nm wavelength filter shows GFP glowing green. This indicates a successful transfection, with cells producing fusion glycosyltransferase proteins. [B] SDS-PAGE gel of concentrated PEI expression media after two and five days of growth. Media was concentrated using a 10 kDa MWCO centrifugal filter, and 11 μ L of concentrates were loaded into each lane. Red box denotes regions where bands of the correct mass are seen. Even though the gel melted during the run, resulting in lanes 10 and 11 being unreadable, positive over expression of the target transferase from the other transfection experiments carried out at the same time suggests that the B4GalT1 expression was successful.

As the expressed glycosyltransferases contain an 8x-His tag on the N-terminal (107), purification and immobilisation of the enzymes can be performed in a single step using Ni-NTA agarose resins. The

resin bound enzymes were packed into the custom-made columns to create the Artificial Golgi Column (AGC). The reaction mixture containing the glycoprotein substrate, donor nucleotide sugars and essential metal co-factor were injected into column with a flow controlled HPLC pump. It is important to note that with a column packing of approximately 200 μL , injection volume of 100 μL and a flow rate of 100 $\mu\text{L}/\text{min}$, the effective enzyme: substrate reaction time is only 2 mins. By calculating by the dead volume of the setup, the reaction mixture was collected from the elution and analysed for glycan proportion changes using PGC-LC-MSMS. Several parameters were tested to create and optimise a working column. These parameters included concentration of co-factor manganese, column material, column internal diameter and amount of glycoprotein substrate added (Figure 16). Once these initial tests were done, further testing was performed; changing the glycoprotein substrate, the glycosyltransferase in the column, and finally combining two separate columns loaded with different glycosyltransferases together in sequence. All tests were performed with a minimum technical replicate of 3 samples, and results are reported as bar graphs of mean + standard deviation.

4.2.4 Initial testing of the B4GalT1-AGC

Initial tests of the B4GalT1-AGC occurred in conditions using low amounts of the essential co-factor for B4GalT1, MnCl_2 (1 mM), to mitigate potential interference between the Mn^{2+} and Ni^{2+} ions. To analyse the change in glycan structures, the relative abundance based on area-under-curve quantitation of extracted ion chromatograms of the precursor glycan and all its product *N*-glycans was calculated. For example, mono-, bi- and tri-galactosylated tri-antennary structures (A3G1, A3G2, and A3G3) were all product glycans from the precursor non-galactosylated tri-antennary *N*-glycan (A3) on the de-sialylated and de-galactosylated fetuin. This means discrepancies between total amounts of *N*-glycan samples are avoided and no one measurement will skew results. While this does not cover all glycan structures of fetuin (also containing bi-antennary (~20%), and incomplete desialylation (A3G1S1 (~11.5%)), it accounts for ~70% of the fetuin glycans, which is representative of the AGC activity.

In Figure 16a, a significant drop of A3 and increase in A3G1 structures is observed when comparing pre-treated Fet -S -G substrate and B4GalT1-AGC treated Fet-S-G product (Sup. Table 2). This initial test in unfavourable co-factor concentrations was performed at a flow rate of 100 $\mu\text{L}/\text{min}$. Subsequent tests of the AGC, including those at 10 mM concentration of MnCl_2 , were performed at 200 $\mu\text{L}/\text{min}$ to increase throughput of experiments. 10 mM of MnCl_2 experiments gave an increased level of galactosylation, significantly increasing the proportion of A3G1, A3G2, and A3G3 *N*-glycans when compared to both controls, and 1 mM MnCl_2 experiments Figure 16a. As 10 mM of MnCl_2 gave significantly improved results, this concentration was used for all other AGC experiments.

4.2.5 Comparing AGC column format

A prototype for the AGC was tested and developed by Dr Moh (PhD thesis) (117). The initial AGC design involved loosely packing 100 μ L of Ni-NTA beads loaded with B4GalT1 into a 1 mL syringe. Substrate flow through this column is gravity dependent and the amount of liquid in the column directly affects the flowrate through the packing. Building upon this working prototype, two of the same syringes were cut in half and attached to each other, creating a column that was able to be connected to a flow-controlled liquid chromatography system (Figure 6). These LC compatible columns proved difficult to mass produce reliably, hence 3D printed columns of defined dimensions were designed (Table 3). Both columns were packed with 200 μ L of B4GalT1 loaded resin and the efficacy of these enzymes was tested (Figure 16).

As shown in Figure 16b, there is no significant difference in results between the home-made syringe columns and 3D printed columns. Relative abundances of all glycans appear similar between columns showing that the 3D printed alternative column is a viable option for subsequent tests.

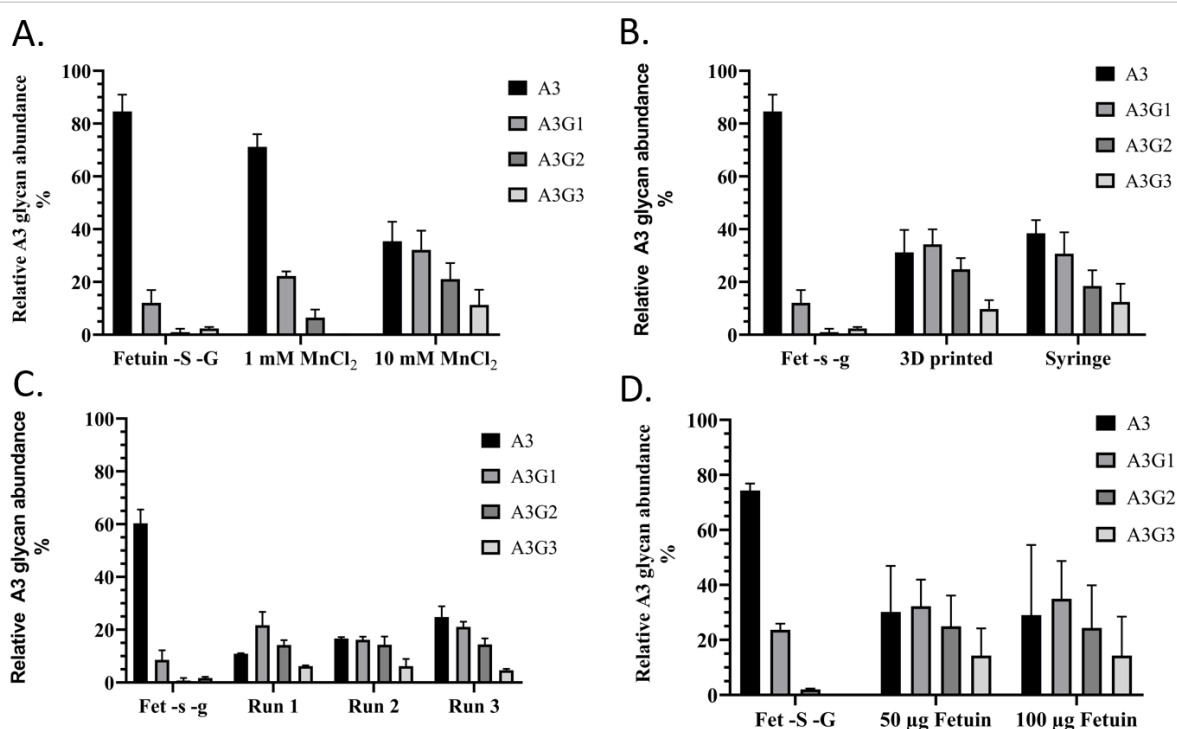


Figure 16 – Initial tests of the B4GalT1-AGC. [A] Varying concentrations of MnCl₂. Including 10 mM of MnCl₂ in reaction mixture results in increased levels of A3G1, A3G2, and A3G3 N-glycan structures (n = 17), and decreased level of A3 N-glycans when compared to both pre-treated fetuin (Fet -S -G) (n = 3) and reaction mixtures containing 1 mM MnCl₂ (n = 3). [B] Relative abundance of A3 glycans present in samples before and after treatment with two different B4GalT1-AGC's. Homemade columns using high-quality syringe plastic (n = 10) are shown to have no substantial difference than those columns made from 3D printed methylacrylic acid ester polymer (n = 7). [C]

Testing the run repeatability of the 4mm I.D. B4GalT1-AGC. A slight decrease in efficiency of ~7% (mean ± SD) is observed as run number increases. n = 9. [D] Testing the glycoprotein capacity of the same 4mm I.D. B4GalT1-AGC with two different amounts of pre-treated fetuin. Both amounts of fetuin added returned the same galactosylation profile, at similar levels (50 µg samples, n = 17; 100 µg tests, n = 11).

4.2.6 Testing the amount of substrate in B4GalT1-AGC activity

To test the capacity of the column, the amount of substrate was increased two-fold (Figure 16). There was no significant difference in the A3 glycoforms of those injections containing 50 µg and those containing 100 µg of pre-treated fetuin (Sup. Table 2). Had the capacity of the column been reached, then the relative amount of *N*-glycan change would have decreased. This implies that the true capacity of protein that the B4GalT1-AGC can act upon in a single injection has not been reached, and further testing with higher amounts of protein is required.

4.2.7 Testing the repeatability of the B4GalT1-AGC activity

To ensure the column efficiency was not degrading over time, sequential runs were performed on the same B4GalT1-AGC (Figure 16c). There was a small difference in the product output between the runs showing that the column has reusability of at least 3 runs. With the change in mean relative abundance between runs of A3 glycan structures (~7 %), a predicted column lifetime of 8 runs was calculated (Efficiency of first run less 7%). This lifetime requires future experimentation to be confirmed. The reusability of the column on a timescale was not tested but is also expected to be a factor in reaction completion.

4.2.8 Adjusting column internal diameter parameters of the B4GalT1-AGC

The difference between a column I.D. of 4 mm and 3mm was tested for the B4GalT1-AGC. By lowering the internal diameter of the column but keeping the amount of packing material the same, the column length of the packing material increases. This increase then corresponds with an increase in the number of theoretical plates present in the column, increasing interaction between substrates in the mobile phase and enzymes in the stationary phase.

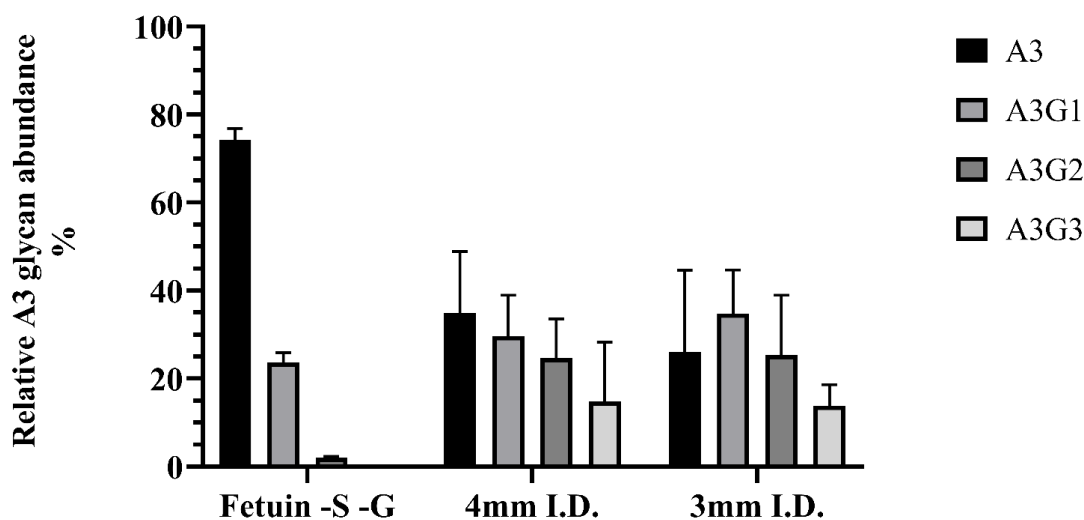


Figure 17 – Comparing a 3mm and 4mm I.D. on column efficiency in the B4GalT1-AGC. No significant difference is observed between the two internal diameters of these columns. Bars shown are mean + SD, with N = 9.

Here, it is observed that whilst there are slight differences between the 3 mm I.D. and 4 mm I.D. B4GalT1-AGC columns on the final completion of galactosylation reaction, these differences do not fall into statistically different significance from one another (Figure 17). As column internal diameter decreases, so does lateral diffusion of all substrates in the mobile phase of the AGC. It can be speculated that this focuses glycoprotein substrates, co-factors, and donor sugars on the same immobilised enzymes, increasing the likelihood that at any one time all three will be in proximity of the same enzyme. It is possible that a change of 1 mm in internal diameter was not sufficient to invoke a noticeable change in reaction completion, despite increasing reaction bed length by a factor of two (~15.67 mm to ~28.00 mm). Alternatively, the sampling methods used resulted in standard error bars that were too large to provide enough resolution for detection of differences between columns.

4.2.9 Testing glycosylation of commercial Trastuzumab in the B4GalT1-AGC

For the AGC to be a useful system it must work on glycoprotein substrates other than fetuin, ideally of high value. Trastuzumab is a valuable therapeutic IgG, with a sale value of USD \$7 052 million in 2016 (18). Fucose-depleted Trastuzumab has been produced in $\Delta FUT8$ CHO cells and found to have greater ADCC as predicted (118). Here, untreated commercial Trastuzumab produced in CHO cells was run through the B4GalT1-AGC in the expectation of galactose addition on FA2 (also commonly referred to as G0F), to FA2G2. Fucosylated bi-antennary structures without galactose residues are the most abundant N-glycan structure on the purchased CHO produced Trastuzumab (90% of total N-glycans), consequently treatment with galactosidase was necessary. Figure 18 shows that the reaction is approximately halfway complete, with tabulated proportions of glycans reflecting this

(Sup. Table 2). Even though *N*-glycans found on Trastuzumab, and IgGs in general, are less accessible than those found on fetuin (Figure 19), the AGC was still effective, converting precursor FA2 (reducing ~70 % to 25 % relative abundance) glycans to the product FA2G1 (increasing 27 % to 42 % relative abundance) and FA2G2 (increasing 3 % to 33 % relative abundance) *N*-glycans (Figure 18, Sup. Table 2).

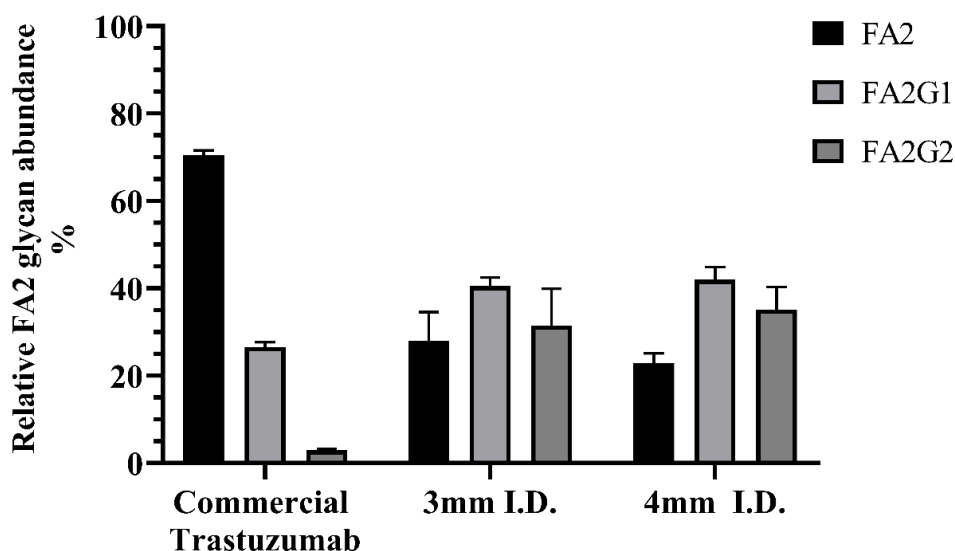


Figure 18 – Testing the *B4GalT1*-AGC with a commercially produced valuable therapeutic, *Trastuzumab*. Existing fucosylated *N*-glycan structures on *Trastuzumab* are ~70 % FA2, and the column was shown to reduce these structures, whilst increasing relative abundance of galactosylated structures FA2G1 and FA2G2 at the same time. Bars shown are mean + SD, with $N = 3$.

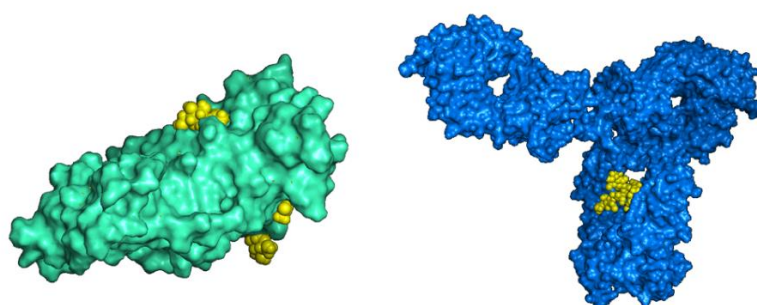


Figure 19 - Crystal structures of mammalian fetuin B PDB:6HPV [Left] (119) and IgG PDB:1HZH [Right] (120). Here *N*-glycan locations are highlighted in yellow. Fetuin *N*-glycans are

exposed on the surface of the protein, whilst IgG N-glycans are shielded by the Fc region of the antibody.

4.2.10 Testing ST6Gal1-GFP AGC with desialylated fetuin as a substrate

The theoretical next step to building a terminal sialic N-glycan was tested, and the B4GalT1-AGC was replaced with an ST6Gal1-GFP-AGC. Fetuin substrates were desialylated with neuraminidase and UDP-galactose replaced with CMP-sialic acid within the experimental reaction mix. All other conditions were unchanged. Preliminary results for this experiment are inconclusive, as whilst there was a trend seen in the decrease in mean relative abundance of A3G3 glycans and an increase in the sialylated products after column interaction the changes are not significant (Figure 20). This may be due to the N-terminus GFP fusion on the enzyme. Further testing and optimisation are required to be done on this recombinantly produced sialyltransferase with and without the GFP fusion in AGC format to confirm its efficiency.

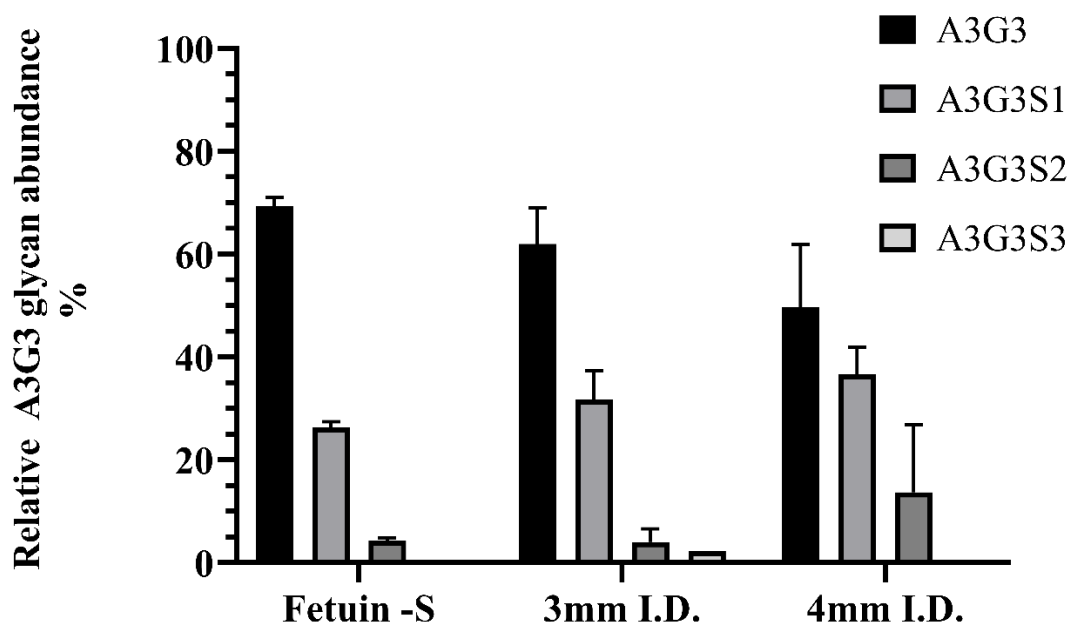


Figure 20 – Testing the ST6Gal1-GFP-AGC with two different internal diameters. Initial experimental results are inconclusive, with sialylation levels increasing but not differing significantly from desialylated fetuin. Bars shown are mean + SD, with N = 9.

4.2.11 B4GalT1-AGC and ST6Gal1-GFP-AGC in sequence

To mimic the trans-Golgi network in the cell, the B4GalT1-AGC and ST6Gal1-GFP-AGC were connected in sequence to perform galactosylation and sialylation in tandem. Fet -S -G was used as the candidate substrate glycoprotein, along with both UDP-Galactose and CMP-Sialic acid required to glycoengineer the predominant A3 structure to an A3G3S3 structure. The B4GalT1-AGC worked with usual efficiency, creating a large proportion of suitable N-glycan precursors synthesised (A3G1,

A3G2, AND A3G3) (Sup. Table 2), for sialic acid addition by the sequential ST6Gal1-GFP-AGC. As previously determined, the ST6Gal1-GFP-AGC results are variable, with large error bars observed (Figure 21). However, although not conclusive, the increase in mono-sialylation of the A3G3 increased structure appeared to correlate with a decrease in its non-sialylated substrate with some appearance of the disialylated product (Sup. Table 2), supporting the success of sequential glycosyltransferase columns.

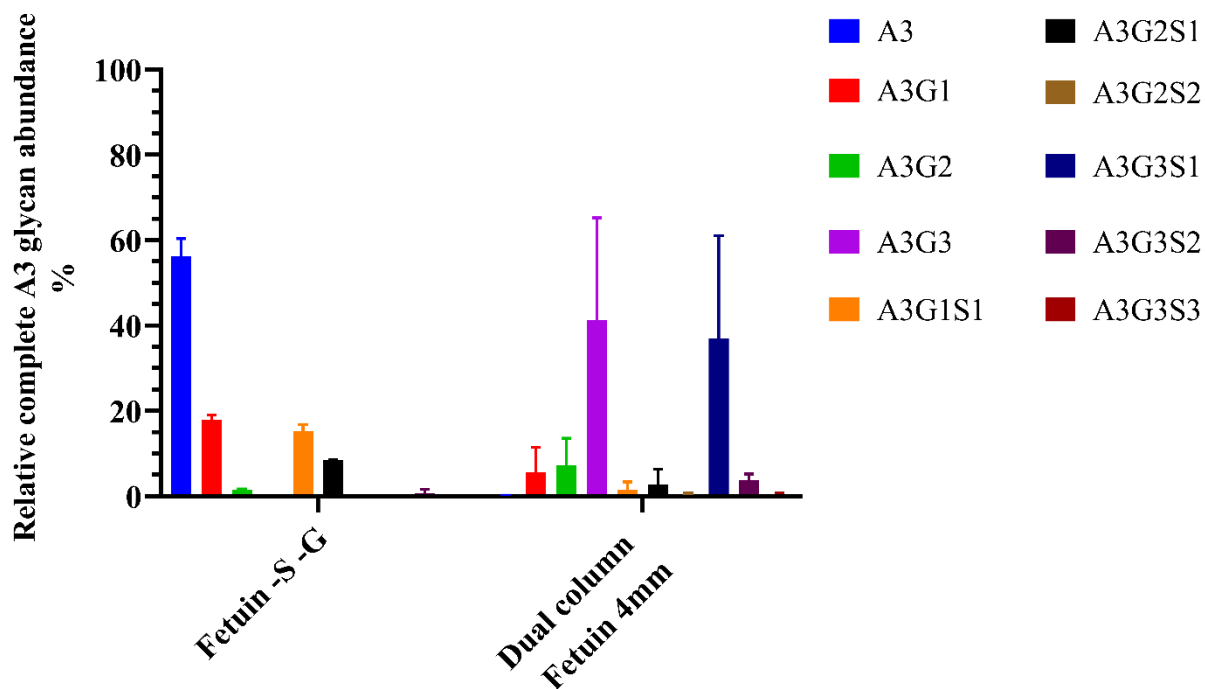


Figure 21 – Comparing the glycoprofile of B4GalT1- and ST6Gal1-GFP- columns connected in sequence. Fet -S -G was used as the substrate glycoprotein, with glycoforms seen to shift to galactosylated and sialylated products. An almost complete loss of A3 structures was indicating complete conversion of substrate. Bars shown are mean + SD, with $N = 3$.

5 Discussion

In this body of work, a minimally engineered *in vivo* production host and a scalable *in vitro* glycosylation system have been developed with the intention of creating a dual glycoengineering system for glycoprotein production that is modular and cost efficient. *In vivo*, an *S. cerevisiae* strain was engineered to produce a mAb (Trastuzumab) with truncated *N*-glycan structures. *In vitro*, a modular AGC was separately designed able to further process the proteins produced in this *S. cerevisiae* strain, potentially transitioning *N*-glycans present to a homogenous human-similar

structure. Having this modular ability *in vitro* at large scale enables the use of one production system to create various glycoforms, reducing strain on resources and need for many individual bioreactors.

As previously stated, STY is an important factor to consider for large-scale production of therapeutics and other valuable proteins (64). Yeast strains such as *S. cerevisiae* or *P. pastoris* excel at this, growing to very high densities while maintaining secretory abilities and eukaryotic protein folding machinery. Here, several genetic engineering techniques such as CRISPR and breeding had been used to create truncated *N*-glycan structures on secreted heterologous proteins, with the final strain able to produce hybrid $\text{Man}_5\text{GlcNAc}_3$ *N*-glycans, once *GnTI* function is confirmed.

A $\text{Man}_5\text{GlcNAc}_2$ *N*-glycan is desirable as with just three steps it can be glycosylated to contain a terminal α -2,6 sialic acid on the 3-arm (Figure 22b), resulting in increased $\text{Fc}\gamma\text{III}$ binding, which gives stronger ADCC activity (121). Terminal mannose residues on the 6-arm will also promote CDC when on mAbs (38), resulting in activation of multiple cellular immune response pathways. As *S. cerevisiae* does not fucosylate *N*-glycans, the increased ADCC activity resultant of an absent core fucose is achieved at the same time. The addition of GlcNAc can be performed either *in vivo* or *in vitro*, by inserting *GnTI* into the *in vivo* model as was performed here, or by immobilising *GnTI* in an AGC. In this manner, the handover point between *in vivo* and *in vitro* systems is flexible and dependent upon cost in the production process.

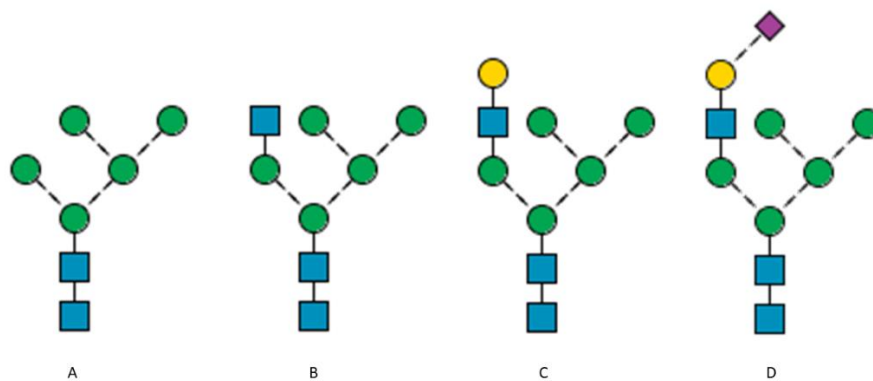


Figure 22 – Produced and targeted *N*-glycan structures. (A) The $\text{Man}_5\text{GlcNAc}_2$ *N*-glycan results from glycoengineering *S. cerevisiae* and is compatible with branch further *GlcNAcylation*; the current handover hybrid *N*-glycan (B) between the *in vivo* host *S. cerevisiae* and *in vitro* AGC system. (C) Galactosylated hybrid glycan: theoretical *N*-glycan after treatment with the *B4GalT1*-AGC. This *N*-glycan is a substrate of the (D) *ST6Gal1*-AGC final *N*-glycan. This structure can be produced in minimally glycoengineered *S. cerevisiae* to produce *N*-glycans with α -2,6-sialylation, lack of a core

fuco, and a high mannose arm resulting in a glycan that theoretically has increased CDC and ADCC activity and is not naturally produced in current production hosts.

There is value in not completely removing lengthy high-mannose glycans from glycoengineered yeast strains. Yeast cell walls contain hypermannosylated glycoproteins, which contribute many cell wall properties. Truncating these structures negatively effects cell wall integrity, limiting growth (122). Our results supported this view, as we found a significant reduction in the optical densities of *OCHI* deleted liquid cultures and smaller colonies (Figure 7) when grown on agar. Growth rate recovery of these strains have been shown to be effective, however this required extensive strain engineering (8, 78). This process is usually time consuming, and yeast strain and growing condition dependant. By limiting the glycoengineering *in vivo*, as demonstrated here, and completing the engineering *in vitro*, it is possible to limit impact on cell viability and concomitant product yields. Coupling a minimally engineered strain to an *in vitro* glycosylation system thereby assists in preventing the need for regenerative strain engineering.

When analysing glycoforms of the generated yeast strains, those containing an *OCHI* deletion appeared as reported in literature, showing an increased abundance in Man₅GlcNAc₂ and Man₈GlcNAc₂ structures (Figure 11) (76, 79, 123). Addition of *MNS1B* resulted in an interesting phenotype, where instead of further mannose trimming as reported in literature (42), an increased abundance of longer Man₉GlcNAc₂ and Man₁₀GlcNAc₂ glycans was observed, with a decreased abundance of Man₈GlcNAc₂ glycans. It is possible that additional glycan trimming activated the UPR pathway (124) and those glycoproteins containing trimmed *N*-glycans were recycled. Another possibility is the *MNS1B* α -1,2-mannosidase produced was correctly working, but other mannosyltransferases such as MNN1 had increased affinity towards the further truncated structures.

Through introduction of a synthetic gene cassette, Trastuzumab was able to be produced in *S. cerevisiae*. Monoclonal antibodies have been introduced into yeast strains previously (15, 59, 80, 125), and shown that IgG peptide chains are correctly folded in yeast (126). The biophysical properties of this yeast derived mAb are still to be determined for stability, substrate affinity and functionality.

The development of an artificial Golgi column is described and contains immobilised glycosyltransferases operating sequentially in a manner which is rapid and controllable. This *in vitro* system is modular and allows for fine-tuning of parameters that are difficult to engineer *in vivo*, such as substrate: enzyme ratio, pH and substrate concentration. Effective galactosylation was observed in both treated fetuin and CHO produced Trastuzumab samples, with a reduction in precursor glycans of up to 50% for fetuin samples (A3) and 42% for Trastuzumab (FA2). The developed B4GalT1-

AGC was shown to be reusable with 12 separate reactions (9 fetuin + 3 Trastuzumab, B4GalT1-AGC) being performed with only a small loss of reactivity (Figure 16). This small loss of reactivity requires further testing to be resolved. The reusability of this column is a critical factor, as while large scale galactosylation reactions have been performed by other researchers who successfully galactosylated 1kg of IgG with 4 g of B4GalT1 over 24 hours (91), the enzymes in this reaction were not recovered. Immobilising enzymes allows for reuse and recycling of glycosyltransferases. As glycosyltransferases are not consumed during reactions, they are only subject to spontaneous degradation. Loss of enzymatic activity can also result in loss of enzymes, which may happen if they leach from their immobilised scaffold. By utilising the 8x His-tag present on the pGEn1 and pGEn2 vectors, an efficient binding system was created for the AGC experiments performed (Figure 14). However, if this binding had proved to be insufficient, the Streptavidin tag also built into the expression vector could have been utilised. The number of enzymes immobilised on the agarose resin used in this work was not calculated, however a common problem for conjugation methods involving physical adsorption or chemical conjugation, such as the method used here, is low coupling yield. The conjugation between glycosyltransferase and resin is an optimisable process, with various solid-binding peptide linkage sequences for different solids being identified for biomolecule conjugation (127).

Experimental observations from this work showed difficulty in consistently producing enzymes for use in the AGC. ST6Gal1 enzymatic efficiency was low (Figure 20). This low activity could be explained by the GFP-fusion tag present at the N-terminus, as the active mechanism for ST6Gal1 involves an N-terminal appendage spanning residues 89-136, which is directly involved in substrate binding (128). The addition of a GFP-fusion on the N-terminus of this enzyme may sterically hinder the conformation required for ST6Gal1 to retain its activity under continuous flow. The presence of the GFP-fusion was still useful however, enabling visual monitoring of transfection and enzyme immobilisation but may not be necessary for the final constructed AGC.

Non-mammalian glycosyltransferases with the ability to carry out identical linkage transfer of sugars is an avenue that has not yet been explored within the AGC. As the AGC is an *in vitro* system, the options for diversifying the final product, how fast this product is made, and its stability are broad, and the original source of enzymes does not matter. This allows bacterial or other high titre expression systems like yeast to be used for enzyme production of AGC's. By moving away from human cells to produce the glycosyltransferases, production scale and cost can be improved. Synthetic and rational enzyme design can also be taken into consideration, designing enzymes with increased stability and activity (129, 130).

Only the most abundant precursor *N*-glycan structure was quantified in this work. It must be remembered that the most abundant *N*-glycan is not the only glycan present on the glycoproteins tested, and other *N*-glycan moieties with compatible precursor structures will also have had their glycans modified. For example, tri-antennary *N*-glycan structures only account for ~70 % of all *N*-glycans present on the fetuin samples tested (Figure 13). Bi-antennary and incompletely desialylated structures such as A3G1S1 were still present in measurable abundance and may have also been subject to galactosylation or sialic addition. Thus, the efficiency of the AGC's tested has only been determined for those most abundant glycans (A3 in fetuin and FA2 in Trastuzumab). The activity of B4GalT1 and ST6Gal1 to specific precursor glycoforms was not considered, and one precursor may be preferentially modified over other glycans (131). The modularity of the AGC becomes effective here, allowing different enzymes that convey the same linkage addition but are more efficient for different precursor glycans to be swapped in as needed.

Chemoenzymatic synthesis of *N*-glycans has previously been shown to be possible through the use of mutated endoglycosidases (86). A key difference between that method and the AGC approach described herein is the use of nucleotide-monosaccharide sugars in the AGC, whereas using mutated Endoglycosidases requires a complete oxazoline-tagged *N*-glycan. Having a modular system allows for more accurate fine-tuning of parameters between reaction columns and gives researchers and pharmaceutical companies an option to create a specific mix of glycoforms. For example, to activate all relevant ADCC and CDC immune pathways for mAbs, different glycoforms are needed. Non-fucosylated, terminally α -2-6 sialylated with a bisecting GlcNAc *N*-glycans can be used to increase ADCC activation, while a hybrid *N*-glycan with either terminal galactose or GlcNAc structures can activate CDC pathways (19). Through future empirical work it may be determined that a specific mix of glycoproteins is ideal for different therapeutic targets. On a purely commercial note, the introduction of the ability to create specific glycoforms of the same protein enables patent development on individual inventions, as each glycoengineered therapeutic will have been made with a different purpose.

6 Conclusion and future directions

In this work, the possibility of combining two separate avenues of glycan engineering was explored. By introducing minimal engineering into an *in vivo* system such as *S. cerevisiae*, and by working towards a high-throughput *in vitro* post-translational modification system in the Artificial Golgi Column, an alternative approach to industrial production of valuable therapeutics is suggested. This approach brings together two existing ideas, resulting in a combined system with high modularity. Through using individual AGC reactors, glycosyltransferases can be swapped as needed in a 'plug

and play' fashion. This plug and play style of glycosylation enables the use of one highly optimised *in vivo* production host, reducing infrastructure and the need for multiple bioreactors. As the final glycosylation system is performed *in vitro*, production hosts from all phyla can be considered, and the capacity to produce human-like glycan structures is no longer a determinant factor in the choice of production host. As such, scalable hosts capable of complex folding such as *S. cerevisiae* and *P. pastoris* become strong contenders in the choice for therapeutic production.

Further optimisation and testing are required to produce Trastuzumab in our engineered strain of *S. cerevisiae*. This work is not unique to Trastuzumab and is required for all therapeutic production strains. Regardless, the use of a high throughput *in vivo* production system capable of producing a therapeutic with a single homogenous precursor is exciting, and with correct implementation non-human, minimally engineered strains may become more ubiquitous throughout industry. For this procedure to be economically viable, all AGC's used in the glycosylation process must proceed with extremely high levels of efficiency, of at least 97% per reaction. This will ensure a sufficient amount of correctly glycosylated glycoprotein substrate is taken to the next stage of modification, without loss of product through partial or incomplete glycosylation.

Further optimisation is required to achieve efficient levels of glycosylation in the AGC. All steps and parts within this system are modular and able to be changed for greater efficiency, with limited effect on the rest of the system. Tests on a larger scale and in higher throughput are also required so that the true capacity of this AGC is found. Currently, preliminary results are promising; commercial Trastuzumab produced by CHO cells with predominant FA2 glycan structure was able to be galactosylated in significant levels using the AGC. With a reaction time of one minute, the implications for therapeutic work and biosimilar research are high. AGC *in vitro* glycosylation also provides opportunities to confer unusual glycans to therapeutic products such as azide-functionalised monosaccharides for biocompatible conjugation (132). Unusual glycans, synthetic glycans, or labelled glycans can now be incorporated into therapeutic products, enabling a host of future testing. On top of using non-mammalian glycosyltransferases, it is also possible to incorporate synthetic transferases that have been designed *in silico*. These proteins could one day be rationally designed and customised for specificity, thermostability, and speed of action.

The future of a dual glycoengineering system is bright, and with further engineering both the *in vivo* and *in vitro* system can be optimised to high efficiency, enabling cheaper therapeutics and faster research into the effects of specific glycoforms.

7 References

1. J. M. Rini, J. D. Esko, "Glycosyltransferases and Glycan-Processing Enzymes" in *Essentials of Glycobiology*, rd *et al.*, Eds. (Cold Spring Harbor Laboratory Press, Copyright 2015-2017 by The Consortium of Glycobiology Editors, La Jolla, California. All rights reserved., Cold Spring Harbor (NY), 2015), 10.1101/glycobiology.3e.006, pp. 65-75.
2. P. Stanley, N. Taniguchi, M. Aebi, "N-Glycans" in *Essentials of Glycobiology*, rd *et al.*, Eds. (Cold Spring Harbor Laboratory Press, Copyright 2015-2017 by The Consortium of Glycobiology Editors, La Jolla, California. All rights reserved., Cold Spring Harbor (NY), 2015), 10.1101/glycobiology.3e.009, pp. 99-111.
3. I. Brockhausen, P. Stanley, "O-GalNAc Glycans" in *Essentials of Glycobiology*, rd *et al.*, Eds. (Cold Spring Harbor Laboratory Press, Copyright 2015-2017 by The Consortium of Glycobiology Editors, La Jolla, California. All rights reserved., Cold Spring Harbor (NY), 2015), 10.1101/glycobiology.3e.010, pp. 113-123.
4. M. Thaysen-Andersen, N. H. Packer, Site-specific glycoproteomics confirms that protein structure dictates formation of N-glycan type, core fucosylation and branching. *Glycobiology* **22**, 1440-1452 (2012).
5. L. Y. Lee, C.-H. Lin, S. Fanayan, N. H. Packer, M. Thaysen-Andersen, Differential Site Accessibility Mechanistically Explains Subcellular-Specific N-Glycosylation Determinants. *Frontiers in Immunology* **5** (2014).
6. F. Higel, A. Seidl, F. Sörgel, W. Friess, N-glycosylation heterogeneity and the influence on structure, function and pharmacokinetics of monoclonal antibodies and Fc fusion proteins. *European Journal of Pharmaceutics and Biopharmaceutics* **100**, 94-100 (2016).
7. R. Jefferis, Recombinant antibody therapeutics: the impact of glycosylation on mechanisms of action. *Trends in Pharmacological Sciences* **30**, 356-362 (2009).
8. A. Beck, O. Cochet, T. Wurch, GlycoFi's technology to control the glycosylation of recombinant therapeutic proteins. *Expert Opinion on Drug Discovery* **5**, 95-111 (2010).
9. G. Walsh, Biopharmaceutical benchmarks 2018. *Nature Biotechnology* **36**, 1136 (2018).
10. K. J. Jeong, S. H. Jang, N. Velmurugan, Recombinant antibodies: engineering and production in yeast and bacterial hosts. *Biotechnol J* **6**, 16-27 (2011).
11. J. M. Smeekens, H. Xiao, R. Wu, Global Analysis of Secreted Proteins and Glycoproteins in *Saccharomyces cerevisiae*. *Journal of Proteome Research* **16**, 1039-1049 (2017).
12. S. Neelamegham *et al.*, Updates to the Symbol Nomenclature for Glycans guidelines. *Glycobiology* **29**, 620-624 (2019).
13. K. W. Moremen, M. Tiemeyer, A. V. Nairn, Vertebrate protein glycosylation: diversity, synthesis and function. *Nature reviews. Molecular cell biology* **13**, 448-462 (2012).
14. N. Dean, Asparagine-linked glycosylation in the yeast Golgi. *Biochimica et Biophysica Acta (BBA) - General Subjects* **1426**, 309-322 (1999).
15. B. Laukens, C. D. Visscher, N. Callewaert, Engineering yeast for producing human glycoproteins: where are we now? *Future Microbiology* **10**, 21-34 (2015).
16. R. Mastrangeli, W. Palinsky, H. Bierau, Glycoengineered antibodies: towards the next-generation of immunotherapeutics. *Glycobiology* **29**, 199-210 (2018).
17. C. W. Lin *et al.*, A common glycan structure on immunoglobulin G for enhancement of effector functions. *Proc Natl Acad Sci U S A* **112**, 10611-10616 (2015).
18. PMLive (2017) Herceptin - Sales performance, data and rankings - Top Pharma List - PMLive. in *Top Pharma List* (GlobalData).
19. A. Russell, E. Adua, I. Ugrina, S. Laws, W. Wang, Unravelling Immunoglobulin G Fc N-Glycosylation: A Dynamic Marker Potentiating Predictive, Preventive and Personalised Medicine. *Int J Mol Sci* **19** (2018).
20. Beneduce C., Kurtagic E., B. C.J., "Anti-inflammatory Activity of IgG-Fc." in *Current Topics in Microbiology and Immunology*. (Springer, Berlin, Heidelberg, 2019), chap. Anti-inflammatory Activity of IgG-Fc.

21. J. N. Arnold, M. R. Wormald, R. B. Sim, P. M. Rudd, R. A. Dwek, The Impact of Glycosylation on the Biological Function and Structure of Human Immunoglobulins. **25**, 21-50 (2007).
22. A. Pincetic *et al.*, Type I and type II Fc receptors regulate innate and adaptive immunity. *Nature Immunology* **15**, 707 (2014).
23. W. I. Weis, M. E. Taylor, K. Drickamer, The C-type lectin superfamily in the immune system. *Immunological Reviews* **163**, 19-34 (1998).
24. C. G. Figdor, Y. van Kooyk, G. J. Adema, C-type lectin receptors on dendritic cells and langerhans cells. *Nature Reviews Immunology* **2**, 77 (2002).
25. Y. Zhao *et al.*, Deletion of core fucosylation on alpha3beta1 integrin down-regulates its functions. *J Biol Chem* **281**, 38343-38350 (2006).
26. J. Lu, P. D. Sun, Structural mechanism of high affinity FcgammaRI recognition of immunoglobulin G. *Immunol Rev* **268**, 192-200 (2015).
27. G. Dekkers *et al.*, Decoding the Human Immunoglobulin G-Glycan Repertoire Reveals a Spectrum of Fc-Receptor- and Complement-Mediated-Effector Activities. *Front Immunol* **8**, 877 (2017).
28. R. L. Shields *et al.*, Lack of fucose on human IgG1 N-linked oligosaccharide improves binding to human Fcgamma RIII and antibody-dependent cellular toxicity. *J Biol Chem* **277**, 26733-26740 (2002).
29. G. P. Subedi, A. W. Barb, The immunoglobulin G1 N-glycan composition affects binding to each low affinity Fc gamma receptor. *MAbs* **8**, 1512-1524 (2016).
30. G. Dekkers *et al.*, Decoding the Human Immunoglobulin G-Glycan Repertoire Reveals a Spectrum of Fc-Receptor- and Complement-Mediated-Effector Activities. *Frontiers in Immunology* **8** (2017).
31. U. Kishore, K. B. Reid, C1q: structure, function, and receptors. *Immunopharmacology* **49**, 159-170 (2000).
32. F. Nimmerjahn, R. M. Anthony, J. V. Ravetch, Agalactosylated IgG antibodies depend on cellular Fc receptors for in vivo activity. *Proc Natl Acad Sci U S A* **104**, 8433-8437 (2007).
33. B. Peschke, C. W. Keller, P. Weber, I. Quast, J. D. Lunemann, Fc-Galactosylation of Human Immunoglobulin Gamma Isotypes Improves C1q Binding and Enhances Complement-Dependent Cytotoxicity. *Front Immunol* **8**, 646 (2017).
34. J. Hodoniczky, Y. Z. Zheng, D. C. James, Control of Recombinant Monoclonal Antibody Effector Functions by Fc N-Glycan Remodeling in Vitro. **21**, 1644-1652 (2005).
35. S. Sha, C. Agarabi, K. Brorson, D.-Y. Lee, S. Yoon, N-Glycosylation Design and Control of Therapeutic Monoclonal Antibodies. *Trends in Biotechnology* **34**, 835-846 (2016).
36. T. S. Raju, Terminal sugars of Fc glycans influence antibody effector functions of IgGs. *Current Opinion in Immunology* **20**, 471-478 (2008).
37. W. Tian *et al.*, The glycosylation design space for recombinant lysosomal replacement enzymes produced in CHO cells. *Nature Communications* **10**, 1785 (2019).
38. K. A. Maupin, D. Liden, B. B. Haab, The fine specificity of mannose-binding and galactose-binding lectins revealed using outlier motif analysis of glycan array data. *Glycobiology* **22**, 160-169 (2012).
39. A. S. More *et al.*, Correlating the Impact of Well-Defined Oligosaccharide Structures on Physical Stability Profiles of IgG1-Fc Glycoforms. *Journal of Pharmaceutical Sciences* **105**, 588-601 (2016).
40. F. Higel *et al.*, N-glycans of complex glycosylated biopharmaceuticals and their impact on protein clearance. *European Journal of Pharmaceutics and Biopharmaceutics* **139**, 123-131 (2019).
41. J. B. Goh, S. K. Ng, Impact of host cell line choice on glycan profile. *Critical Reviews in Biotechnology* **38**, 851-867 (2018).
42. W. Vervecken *et al.*, In Vivo Synthesis of Mammalian-Like, Hybrid-Type N-Glycans in *Pichia pastoris*. *Applied and Environmental Microbiology* **70**, 2639-2646 (2004).

43. K. De Pourcq, K. De Schutter, N. J. A. M. Callewaert, Biotechnology, Engineering of glycosylation in yeast and other fungi: current state and perspectives. *Applied Microbial Biotechnology* **87**, 1617-1631 (2010).
44. I. Fitzgerald, B. S. J. M. C. F. Glick, Secretion of a foreign protein from budding yeasts is enhanced by cotranslational translocation and by suppression of vacuolar targeting. *Microbial Cell Factories* **13**, 125 (2014).
45. Y. Zhou, R. Raju, C. Alves, A. Gilbert, Debottlenecking protein secretion and reducing protein aggregation in the cellular host. *Current Opinion in Biotechnology* **53**, 151-157 (2018).
46. G. P. Subedi, R. W. Johnson, H. A. Moniz, K. W. Moremen, A. Barb, High Yield Expression of Recombinant Human Proteins with the Transient Transfection of HEK293 Cells in Suspension. *Journal of visualized experiments : JoVE* 10.3791/53568, e53568-e53568 (2015).
47. L.-X. Wang, X. Tong, C. Li, J. P. Giddens, T. Li, Glycoengineering of Antibodies for Modulating Functions. *Annual Review of Biochemistry* 10.1146/annurev-biochem-062917-012911 (2019).
48. A. Croset *et al.*, Differences in the glycosylation of recombinant proteins expressed in HEK and CHO cells. *Journal of Biotechnology* **161**, 336-348 (2012).
49. E. Böhm *et al.*, Differences in N-glycosylation of recombinant human coagulation factor VII derived from BHK, CHO, and HEK293 cells. *BMC Biotechnology* **15**, 87 (2015).
50. F. N. Lamari, N. K. Karamanos, Separation methods for sialic acids and critical evaluation of their biologic relevance. *J Chromatogr B Analyt Technol Biomed Life Sci* **781**, 3-19 (2002).
51. M. C. Borys *et al.*, Effects of culture conditions on N-glycolylneuraminic acid (Neu5Gc) content of a recombinant fusion protein produced in CHO cells. *Biotechnology and Bioengineering* **105**, 1048-1057 (2010).
52. A. R. Fleisher, J. Marzowski, W. C. Wang, H. V. Raff, Fluorophore-labeled carbohydrate analysis of immunoglobulin fusion proteins: Correlation of oligosaccharide content with in vivo clearance profile. *Biotechnol Bioeng* **46**, 399-407 (1995).
53. M. Hedlund, V. Padler-Karavani, N. M. Varki, A. Varki, Evidence for a human-specific mechanism for diet and antibody-mediated inflammation in carcinoma progression. *Proceedings of the National Academy of Sciences* **105**, 18936-18941 (2008).
54. T. Pham *et al.*, Evidence for a novel human-specific xeno-auto-antibody response against vascular endothelium. *Blood* **114**, 5225-5235 (2009).
55. N. K. Tripathi, Production and Purification of Recombinant Proteins from Escherichia coli. *ChemBioEng Reviews* **3**, 116-133 (2016).
56. C. J. Huang, H. Lin, X. Yang, Industrial production of recombinant therapeutics in Escherichia coli and its recent advancements. *J Ind Microbiol Biotechnol* **39**, 383-399 (2012).
57. H. Nausch *et al.*, Recombinant production of human interleukin 6 in Escherichia coli. *PLoS One* **8**, e54933 (2013).
58. M. Wacker *et al.*, N-Linked Glycosylation in Campylobacter jejuni and Its Functional Transfer into E. coli. *Science* **298**, 1790-1793 (2002).
59. J. Kaur, A. Kumar, J. Kaur, Strategies for optimization of heterologous protein expression in E. coli: Roadblocks and reinforcements. *International Journal of Biological Macromolecules* **106**, 803-822 (2018).
60. J. A. Wayman, C. Glasscock, T. J. Mansell, M. P. DeLisa, J. D. Varner, Improving designer glycan production in Escherichia coli through model-guided metabolic engineering. *Metabolic Engineering Communications* **9**, e00088 (2019).
61. A. M.-P. Fuentes *et al.*, Expression Atlas: gene and protein expression across multiple studies and organisms. *Nucleic Acids Research* **46**, D246-D251 (2017).

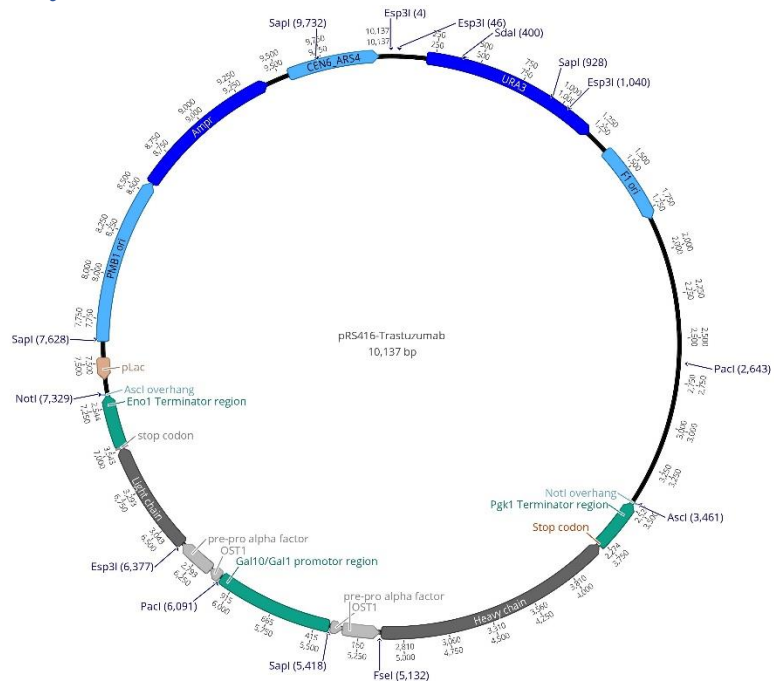
62. J. C. de Ruijter, E. V. Koskela, A. D. J. M. C. F. Frey, Enhancing antibody folding and secretion by tailoring the *Saccharomyces cerevisiae* endoplasmic reticulum. **15**, 87 (2016).
63. M. Ilmén *et al.*, High level secretion of cellobiohydrolases by *Saccharomyces cerevisiae*. *Biotechnology for Biofuels* **4**, 30 (2011).
64. M. A. Piirainen, H. Boer, J. C. de Ruijter, A. D. Frey, A dual approach for improving homogeneity of a human-type N-glycan structure in *Saccharomyces cerevisiae*. *Glycoconjugate Journal* **33**, 189-199 (2016).
65. M. A. Piirainen, H. Salminen, A. D. Frey, "Tailoring N-Glycan Biosynthesis for Production of Therapeutic Proteins in *Saccharomyces cerevisiae*" in *Recombinant Protein Production in Yeast*, B. Gasser, D. Mattanovich, Eds. (Springer New York, New York, NY, 2019), 10.1007/978-1-4939-9024-5_10, pp. 227-241.
66. F. Parsaie Nasab, M. Aebi, G. Bernhard, A. D. Frey, A Combined System for Engineering Glycosylation Efficiency and Glycan Structure in *Saccharomyces cerevisiae*. *Applied and Environmental Microbiology* **79**, 997 (2013).
67. D. Sleep *et al.*, *Saccharomyces Cerevisiae* Strains that Overexpress Heterologous Proteins. *Bio/Technology* **9**, 183-187 (1991).
68. J. Klumperman, Architecture of the mammalian Golgi. *Cold Spring Harbor perspectives in biology* **3** (2011).
69. O. W. Rossanese *et al.*, Golgi Structure Correlates with Transitional Endoplasmic Reticulum Organization in *Pichia pastoris* and *Saccharomyces cerevisiae*. *The Journal of Cell Biology* **145**, 69 (1999).
70. A. Maccani *et al.*, *Pichia pastoris* secretes recombinant proteins less efficiently than Chinese hamster ovary cells but allows higher space-time yields for less complex proteins. **9** (2014).
71. R. A. Darby, S. P. Cartwright, M. V. Dilworth, R. M. Bill, Which yeast species shall I choose? *Saccharomyces cerevisiae* versus *Pichia pastoris* (review). *Methods Mol Biol* **866**, 11-23 (2012).
72. W. J. Holmes, R. A. J. Darby, M. D. B. Wilks, R. Smith, R. M. Bill, Developing a scalable model of recombinant protein yield from *Pichia pastoris*: the influence of culture conditions, biomass and induction regime. *Microbial Cell Factories* **8**, 35 (2009).
73. J. M. Cregg, T. S. Vedvick, W. C. Raschke, Recent advances in the expression of foreign genes in *Pichia pastoris*. *Bio/technology (Nature Publishing Company)* **11**, 905-910 (1993).
74. T. Nagasu *et al.*, Isolation of new temperature-sensitive mutants of *Saccharomyces cerevisiae* deficient in mannose outer chain elongation. *Yeast* **8**, 535-547 (1992).
75. B. K. Choi *et al.*, Use of combinatorial genetic libraries to humanize N-linked glycosylation in the yeast *Pichia pastoris*. *Proc Natl Acad Sci U S A* **100**, 5022-5027 (2003).
76. Y. Chiba *et al.*, Production of human compatible high mannose-type (Man5GlcNAc2) sugar chains in *Saccharomyces cerevisiae*. *J Biol Chem* **273**, 26298-26304 (1998).
77. W. Chotigeat, W. Chayanunnukul, A. Phongdara, Expression of a mammalian α 2,6-sialyltransferase gene in *Pichia pastoris*. *Journal of Biotechnology* **81**, 55-61 (2000).
79. H. Abe *et al.*, Development of valuable yeast strains using a novel mutagenesis technique for the effective production of therapeutic glycoproteins. *Glycobiology* **19**, 428-436 (2009).
80. C. De Wachter, L. Van Landuyt, N. Callewaert, "Engineering of Yeast Glycoprotein Expression" in *Advances in Biochemical Engineering/Biotechnology*. (Springer, Berlin, Heidelberg, 2018), https://doi.org/10.1007/10_2018_69.
81. C.-P. Liu *et al.*, Glycoengineering of antibody (Herceptin) through yeast expression and in vitro enzymatic glycosylation. *Proc Natl Acad Sci USA* **115**, 720-725 (2018).
82. D. Mattanovich, M. Sauer, B. J. M. C. F. Gasser, Yeast biotechnology: teaching the old dog new tricks. **13** (2014).
83. K. R. Love, N. C. Dalvie, J. C. Love, The yeast stands alone: the future of protein biologic production. *Current Opinion in Biotechnology* **53**, 50-58 (2018).

84. C. Sheridan, Commercial interest grows in glycan analysis. *Nat Biotechnol* **25**, 145-146 (2007).
85. S.-Q. Fan, W. Huang, L.-X. Wang, Remarkable Transglycosylation Activity of Glycosynthase Mutants of Endo-D, an Endo- β -N-acetylglucosaminidase from *Streptococcus pneumoniae*. *Journal of Biological Chemistry* **287**, 11272-11281 (2012).
86. J. P. Giddens, J. V. Lomino, D. J. DiLillo, J. V. Ravetch, L.-X. Wang, Site-selective chemoenzymatic glycoengineering of Fab and Fc glycans of a therapeutic antibody. *Proceedings of the National Academy of Sciences* **115**, 12023-12027 (2018).
87. W. Huang, J. Giddens, S.-Q. Fan, C. Toonstra, L.-X. Wang, Chemoenzymatic Glycoengineering of Intact IgG Antibodies for Gain of Functions. *Journal of the American Chemical Society* **134**, 12308-12318 (2012).
88. C. M. Karsten *et al.*, Anti-inflammatory activity of IgG1 mediated by Fc galactosylation and association of Fc γ RIIB and dectin-1. *Nature medicine* **18**, 1401-1406 (2012).
89. J. Hodoniczky, Y. Z. Zheng, D. C. James, Control of recombinant monoclonal antibody effector functions by Fc N-glycan remodeling in vitro. *Biotechnol Prog* **21**, 1644-1652 (2005).
90. M. Kurogochi *et al.*, Glycoengineered Monoclonal Antibodies with Homogeneous Glycan (M3, G0, G2, and A2) Using a Chemoenzymatic Approach Have Different Affinities for Fc γ RIIIa and Variable Antibody-Dependent Cellular Cytotoxicity Activities. *PLOS ONE* **10**, e0132848 (2015).
91. T. S. Raju, J. B. Briggs, S. M. Chamow, M. E. Winkler, A. J. Jones, Glycoengineering of therapeutic glycoproteins: in vitro galactosylation and sialylation of glycoproteins with terminal N-acetylglucosamine and galactose residues. *Biochemistry* **40**, 8868-8876 (2001).
92. D. Warnock *et al.*, In vitro galactosylation of human IgG at 1 kg scale using recombinant galactosyltransferase. *Biotechnology and Bioengineering* **92**, 831-842 (2005).
93. M. Thomann *et al.*, In vitro glycoengineering of IgG1 and its effect on Fc receptor binding and ADCC activity. *PLoS One* **10**, e0134949 (2015).
94. L. Cao, L. v. Langen, R. A. Sheldon, Immobilised enzymes: carrier-bound or carrier-free? *Current Opinion in Biotechnology* **14**, 387-394 (2003).
95. S. Daniel *et al.*, Golgi-on-a-Chip for the Cell-Free Bio-Nanomanufacturing of Protein Therapeutics. *Biophysical Journal* **116**, 1a (2019).
96. T. H. Li *et al.*, An automated platform for the enzyme-mediated assembly of complex oligosaccharides. *Nat. Chem.* **11**, 229-236 (2019).
97. L. Liu *et al.*, Streamlining the chemoenzymatic synthesis of complex N-glycans by a stop and go strategy. *Nat. Chem.* **11**, 161-169 (2019).
98. K. Petroll, D. Kopp, A. Care, P. L. Bergquist, A. Sunna, Tools and strategies for constructing cell-free enzyme pathways. *Biotechnology Advances* **37**, 91-108 (2019).
99. A. Care, K. Petroll, E. S. Y. Gibson, P. L. Bergquist, A. Sunna, Solid-binding peptides for immobilisation of thermostable enzymes to hydrolyse biomass polysaccharides. *Biotechnology for Biofuels* **10**, 29 (2017).
100. J. G. Martin *et al.*, Toward an Artificial Golgi: Redesigning the Biological Activities of Heparan Sulfate on a Digital Microfluidic Chip. *Journal of the American Chemical Society* **131**, 11041-11048 (2009).
101. O. V. Klymenko, N. Shah, C. Kontoravdi, K. E. Royle, K. M. Polizzi, Designing an Artificial Golgi reactor to achieve targeted glycosylation of monoclonal antibodies. *AIChE* **62**, 2959-2973 (2016).
102. C. Geisler, H. Mabashi-Asazuma, C.-W. Kuo, K.-H. Khoo, D. L. Jarvis, Engineering β 1,4-galactosyltransferase I to reduce secretion and enhance N-glycan elongation in insect cells. *Journal of Biotechnology* **193**, 52-65 (2015).
103. C. B. Brachmann *et al.*, Designer deletion strains derived from *Saccharomyces cerevisiae* S288C: a useful set of strains and plasmids for PCR-mediated gene disruption and other applications. *Yeast* **14**, 115-132 (1998).

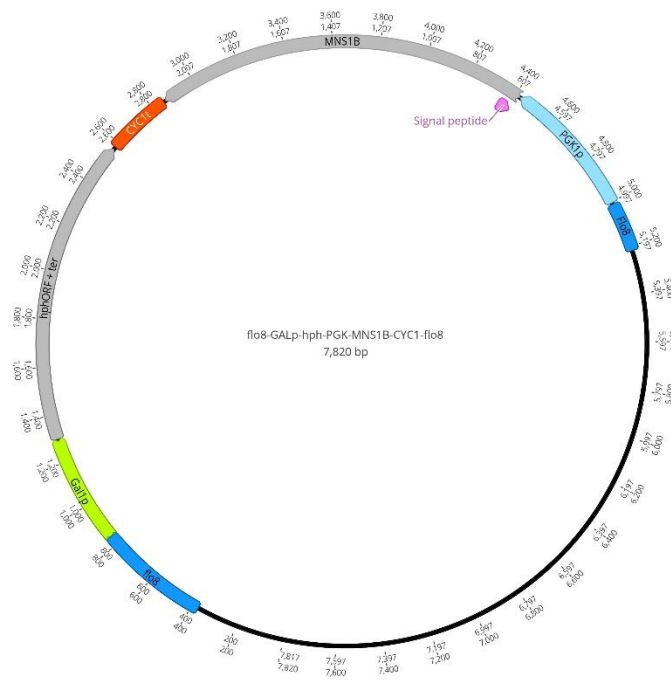
104. G. Giaever, C. Nislow, The Yeast Deletion Collection: A Decade of Functional Genomics. *Genetics* **197**, 451-465 (2014).
105. M. Lööke, K. Kristjuhan, A. Kristjuhan, Extraction of genomic DNA from yeasts for PCR-based applications. *BioTechniques* **50**, 325-328 (2011).
106. M. R. Green, J. Sambrook, *Molecular Cloning: A Laboratory Manual* (Cold Spring Harbor Laboratory Press, 2012).
107. J. Hill, K. A. Donald, D. E. Griffiths, DMSO-enhanced whole cell yeast transformation. *Nucleic acids research* **19**, 5791-5791 (1991).
108. A. Sharma *et al.*, DNASU plasmid and PSI: Biology-Materials repositories: resources to accelerate biological research. *Nucleic Acids Research* **42**, D1253-D1260 (2013).
109. G. P. Au - Subedi, R. W. Au - Johnson, H. A. Au - Moniz, K. W. Au - Moremen, A. Au - Barb, High Yield Expression of Recombinant Human Proteins with the Transient Transfection of HEK293 Cells in Suspension. *JoVE* doi:10.3791/53568, e53568 (2015).
110. J.-D. Pédelacq, S. Cabantous, T. Tran, T. C. Terwilliger, G. S. Waldo, Engineering and characterization of a superfolder green fluorescent protein. *Nature Biotechnology* **24**, 79-88 (2006).
111. P. H. Jensen, N. G. Karlsson, D. Kolarich, N. H. Packer, Structural analysis of N- and O-glycans released from glycoproteins. *Nature Protocols* **7**, 1299 (2012).
112. H. Hinneburg *et al.*, Post-Column Make-Up Flow (PCMF) Enhances the Performance of Capillary-Flow PGC-LC-MS/MS-Based Glycomics. *Anal Chem* **91**, 4559-4567 (2019).
113. B. MacLean *et al.*, Skyline: an open source document editor for creating and analyzing targeted proteomics experiments. *Bioinformatics* **26**, 966-968 (2010).
114. M. L. Swift, GraphPad Prism, Data Analysis, and Scientific Graphing. *Journal of Chemical Information and Computer Sciences* **37**, 411-412 (1997).
115. H. Tang *et al.*, N-hypermannose glycosylation disruption enhances recombinant protein production by regulating secretory pathway and cell wall integrity in *Saccharomyces cerevisiae*. *Scientific Reports* **6**, 25654 (2016).
116. Y. H. Kim *et al.*, Abolishment of N-glycan mannosylphosphorylation in glyco-engineered *Saccharomyces cerevisiae* by double disruption of *MNN4* and *MNN14* genes. *Applied Microbial Biotechnology* **101**, 2979-2989 (2017).
117. R. Kumar, J. Yang, R. D. Larsen, P. Stanley, Cloning and expression of N-acetylglucosaminyltransferase I, the medial Golgi transferase that initiates complex N-linked carbohydrate formation. *Proc Natl Acad Sci U S A* **87**, 9948-9952 (1990).
118. E. S. X. Moh (2018) Platforms for *In Vitro* Glycoengineering of proteins. in *Department of Chemistry and Biomolecular Sciences* (Macquarie University, Sydney, Australia), p 157.
119. J. J. Listinsky, G. P. Siegal, C. M. Listinsky, Glycoengineering in cancer therapeutics: a review with fucose-depleted trastuzumab as the model. *Anti-Cancer Drugs* **24**, 219-227 (2013).
120. A. Cuppari *et al.*, Structure of mammalian plasma fetuin-B and its mechanism of selective metalloproteinase inhibition. *IUCrJ* **6**, 317-330 (2019).
121. E. O. Saphire *et al.*, Crystal structure of a neutralizing human IGG against HIV-1: a template for vaccine design. *Science* **293**, 1155-1159 (2001).
122. C.-W. Lin *et al.*, A common glycan structure on immunoglobulin G for enhancement of effector functions. *Proceedings of the National Academy of Sciences* **112**, 10611-10616 (2015).
123. K. Nakayama, T. Nagasu, Y. Shimma, J. Kuromitsu, Y. Jigami, *OCH1* encodes a novel membrane bound mannosyltransferase: outer chain elongation of asparagine-linked oligosaccharides. *The EMBO Journal* **11**, 2511-2519 (1992).
124. J. Ye *et al.*, Optimization of a glycoengineered *Pichia pastoris* cultivation process for commercial antibody production. *Cell Culture and Tissue Engineering* **27**, 1744-1750 (2011).

125. P. Walter, D. Ron, The Unfolded Protein Response: From Stress Pathway to Homeostatic Regulation. *Science* **334**, 1081-1086 (2011).
126. E. Gecchele *et al.*, A comparative analysis of recombinant protein expression in different biofactories: bacteria, insect cells and plant systems. *Journal of visualized experiments : JoVE* 10.3791/52459, 52459 (2015).
127. M. Vanhove, Y. K. Usherwood, L. M. J. I. Hendershot, Unassembled Ig heavy chains do not cycle from BiP in vivo but require light chains to trigger their release. **15** (2001).
128. A. Care, P. L. Bergquist, A. Sunna, "Solid-Binding Peptides in Biomedicine" in *Peptides and Peptide-based Biomaterials and their Biomedical Applications*, A. Sunna, A. Care, P. L. Bergquist, Eds. (Springer International Publishing, Cham, 2017), 10.1007/978-3-319-66095-0_2, pp. 21-36.
129. B. Kuhn *et al.*, The structure of human alpha-2,6-sialyltransferase reveals the binding mode of complex glycans. *Acta Crystallogr D Biol Crystallogr* **69**, 1826-1838 (2013).
130. M. A. Longo, D. Combes, Thermostability of modified enzymes: a detailed study. *Journal of Chemical Technology & Biotechnology* **74**, 25-32 (1999).
131. G. T. Beckham *et al.*, Harnessing glycosylation to improve cellulase activity. *Current Opinion in Biotechnology* **23**, 338-345 (2012).
132. T. Hennet, The galactosyltransferase family. *Cellular and Molecular Life Sciences CMLS* **59**, 1081-1095 (2002).
133. E. S. X. Moh, N. Sayyadi, N. H. Packer, Chemoenzymatic glycan labelling as a platform for site-specific IgM-antibody drug conjugates. *Analytical Biochemistry* **584**, 113385 (2019).

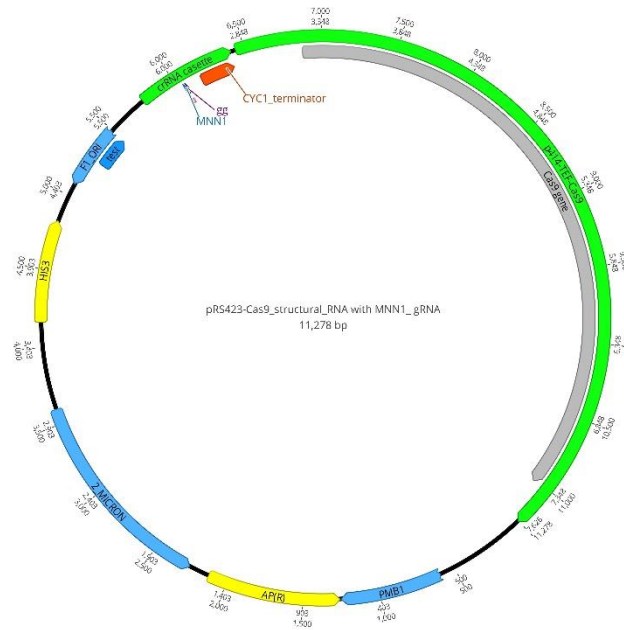
8 Supplementary material



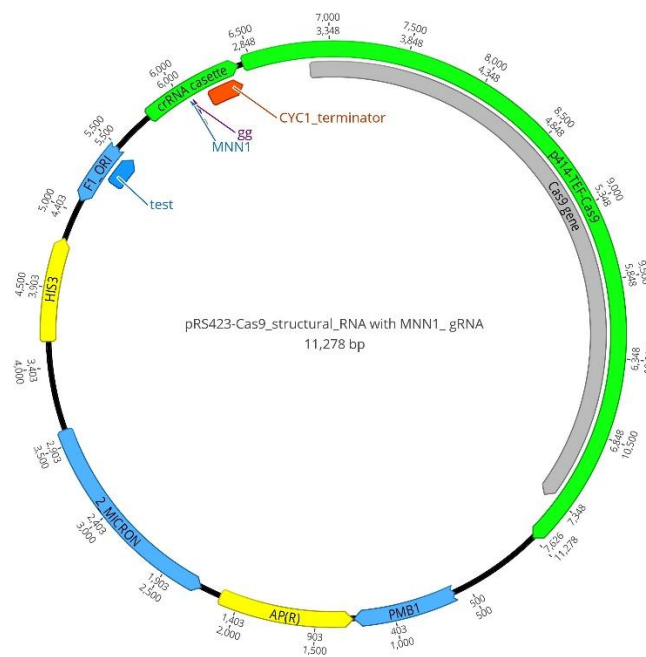
Supplementary Figure 1 - Visual representation of the Trastuzumab expression vector.



Supplementary Figure 2 – Expression vector for FLO8 integrative plasmid of α -1,2-mannosidase (MNS1B). hphORF denotes a hygromycin resistance gene, induced under presence of galactose.



Supplementary Figure 3 – Expression vector for CRISPR/Cas9 plasmid, containing MNN1 specific PAM sequence.



Supplementary Figure 4 – Visual representation of MNN1 specific CRISPR expression vector.

Supplementary Table 1 – Primer sequences used throughout experiments performed.

| <i>Primer</i> | <i>5' to 3' sequence</i> |
|--|---|
| <i>MNN14 flanking region - forward</i> | GGGCCTATTTCTACTTTGGGG |
| <i>MNN14 flanking region - reverse</i> | CGTAAGGGCCGAATTTAAGTGA |
| <i>OCH1 flanking region - forward</i> | CCCATCTGCATCCTTTTATATTTAATAG |
| <i>OCH1 flanking region - reverse</i> | GGGTATGATGAAAGGAGAGC |
| <i>MNN1 flanking region - forward</i> | TACTCTCGAAAAACGTAATCTTGCG |
| <i>MNN1 flanking region - reverse</i> | CCGATATGCTTTACTATACATGTTCA |
| <i>MNN4 flanking region - forward</i> | GTATAATTACCACGATTCCGTC |
| <i>MNN4 flanking region - forward</i> | CGTGGCTTCAAATTTGATATC |
| <i>MNN1 amplicon for CRISPR gRNA - forward</i> | AGTTCGATCATAAACTGGTGTTTTAGAGCTAGAAATAGCAAG |
| <i>MNN1 amplicon for CRISPR gRNA - reverse</i> | ACCAGTTTTATGATCGAACTGATCATTTATCTTTCCTGCG |
| <i>GnTI amplicon with MNN1 flanking tail - forward</i> | ATGTTGGCACTCCGGAGATTTATATTAACCAAAGGTCTTTGCGATCGCTC CCTCCTTCT |
| <i>GnTI amplicon with MNN1 flanking tail - reverse</i> | CTAGCTTTGTTTCGTGTCTAGAATTTTCTAATTCCTTGATCTAAATGGTTCC AAGGCCGGC |

Primer 5' to 3' sequence

Internal α -1,2-mannosidase - forward ACACCACCTACGCTGACTTG

Internal α -1,2-mannosidase - reverse CGTTAGCAGCGTTAACGTCG

Internal GnTI - forward AAGGCTTTCTGGGACGACTG

Internal GnTI - reverse GTGGTTCCAAGATGGGTCGT

Supplementary Table 2 – Degrees of change resulting from treatment with the AGC.

| | % | SD | n | % | SD | n | % | SD | n | % | SD | n |
|--|-----------|------|----|-------------|------|----|-------------|------|----|-------------|------|----|
| 3D printed column vs syringe column | | | | | | | | | | | | |
| | <i>A3</i> | | | <i>A3G1</i> | | | <i>A3G2</i> | | | <i>A3G3</i> | | |
| Fetuin -S -G | 84.60 | 6.37 | 3 | 12.07 | 4.85 | 3 | 0.98 | 1.30 | 3 | 2.34 | 0.58 | 3 |
| 3D printed | 31.19 | 8.51 | 7 | 34.24 | 5.66 | 7 | 24.82 | 4.21 | 7 | 9.75 | 3.32 | 7 |
| Syringe | 38.40 | 5.02 | 10 | 30.71 | 8.12 | 10 | 18.48 | 5.94 | 10 | 12.41 | 6.92 | 10 |
| Changing concentrations of MnCl₂ | | | | | | | | | | | | |
| | <i>A3</i> | | | <i>A3G1</i> | | | <i>A3G2</i> | | | <i>A3G3</i> | | |
| Fetuin -S -G | 84.60 | 6.37 | 3 | 12.07 | 4.85 | 3 | 0.98 | 1.30 | 3 | 2.34 | 0.58 | 3 |
| 1 mM MnCl₂ | 71.19 | 4.78 | 3 | 22.23 | 1.72 | 3 | 6.45 | 3.08 | 3 | 0.14 | 0.05 | 3 |
| 10 mM MnCl₂ | 35.43 | 7.40 | 17 | 32.16 | 7.23 | 17 | 21.09 | 6.07 | 17 | 11.32 | 5.74 | 17 |
| Repeatability of B4GalT1 AGC | | | | | | | | | | | | |
| | <i>A3</i> | | | <i>A3G1</i> | | | <i>A3G2</i> | | | <i>A3G3</i> | | |
| Fetuin -S -G | 60.32 | 5.19 | 3 | 8.61 | 3.56 | 3 | 0.72 | 0.97 | 3 | 1.67 | 0.46 | 3 |

| | % | SD | n | % | SD | n | % | SD | n | % | SD | n |
|--|-------------|-------|----|---------------|-------|----|---------------|-------|----|---------------|-------|-----|
| Run 1 | 10.94 | 0.17 | 2 | 21.71 | 5.06 | 2 | 14.17 | 1.88 | 2 | 6.22 | 0.28 | 2 |
| Run 2 | 16.63 | 0.59 | 2 | 16.18 | 1.17 | 2 | 14.28 | 3.10 | 2 | 6.20 | 2.69 | 2 |
| Run 3 | 24.79 | 4.08 | 3 | 21.08 | 1.95 | 3 | 14.41 | 2.27 | 3 | 4.61 | 0.54 | 3 |
| 4mm I.D. vs 3mm I.D | | | | | | | | | | | | |
| | <i>A3</i> | | | <i>A3G1</i> | | | <i>A3G2</i> | | | <i>A3G3</i> | | |
| Fetuin -S -G | 74.31 | 2.57 | 2 | 23.69 | 2.25 | 2 | 2.01 | 0.32 | 2 | N/A | N/A | N/A |
| 4mm I.D. | 34.84 | 14.10 | 8 | 29.67 | 9.25 | 9 | 24.64 | 8.93 | 9 | 14.73 | 13.58 | 9 |
| 3mm I.D. | 26.06 | 18.55 | 9 | 34.80 | 9.89 | 9 | 25.30 | 13.59 | 9 | 13.84 | 4.80 | 9 |
| Changing amounts of protein added to AGC | | | | | | | | | | | | |
| | <i>A3</i> | | | <i>A3G1</i> | | | <i>A3G2</i> | | | <i>A3G3</i> | | |
| Fetuin -S -G | 74.31 | 2.57 | 2 | 23.69 | 2.25 | 2 | 2.01 | 0.32 | 2 | | | |
| 50 µg Fetuin | 30.19 | 16.71 | 17 | 32.23 | 9.66 | 18 | 24.97 | 11.16 | 18 | 14.28 | 9.89 | 18 |
| 100 µg Fetuin | 29.02 | 25.53 | 11 | 34.96 | 13.71 | 11 | 24.38 | 15.50 | 11 | 14.32 | 14.17 | 9 |
| Commercial Trastuzumab in the B4GalT1 AGC | | | | | | | | | | | | |
| | <i>FA2</i> | | | <i>FA2G1</i> | | | <i>FA2G2</i> | | | | | |
| Comm. Tmab | 70.40 | 1.15 | 3 | 26.61 | 1.10 | 3 | 3.00 | 0.23 | 3 | | | |
| 3mm I.D. | 27.97 | 6.62 | 3 | 40.55 | 1.93 | 3 | 31.48 | 8.43 | 3 | | | |
| 4mm I.D. | 32.29 | 16.42 | 3 | 42.00 | 2.87 | 2 | 35.15 | 5.16 | 3 | | | |
| Fetuin in the ST6Gal1-GFP AGC | | | | | | | | | | | | |
| | <i>A3G3</i> | | | <i>A3G3S1</i> | | | <i>A3G3S2</i> | | | <i>A3G3S3</i> | | |
| Fetuin -S | 69.37 | 1.64 | 2 | 26.37 | 1.02 | 2 | 4.25 | 0.62 | 2 | 0.00 | 0.00 | 2 |
| 3mm I.D. | 61.96 | 6.99 | 9 | 31.74 | 5.54 | 9 | 4.05 | 2.51 | 9 | 2.25 | 1.64 | 9 |

| | % | SD | n | % | SD | n | % | SD | n | % | SD | n |
|---|---------------|-------|---|---------------|------|---|---------------|-------|---|---------------|-------|---|
| 4mm I.D. | 49.73 | 12.12 | 9 | 36.57 | 5.27 | 9 | 13.70 | 13.15 | 9 | 0.00 | 0.00 | 9 |
| Fetuin in the B4GalT1 ST6Gal1-GFP AGC | | | | | | | | | | | | |
| | <i>A3</i> | | | <i>A3G1</i> | | | <i>A3G2</i> | | | <i>A3G3</i> | | |
| Fetuin -S -G | 56.33 | 4.04 | 2 | 17.91 | 1.03 | 2 | 1.52 | 0.19 | 2 | 0.00 | 0.00 | 2 |
| Fetuin -S | 0.20 | 0.14 | 2 | 0.25 | 0.02 | 2 | 2.12 | 0.29 | 2 | 66.07 | 11.94 | 2 |
| Dual column | 0.13 | 0.13 | 3 | 5.56 | 5.88 | 3 | 7.20 | 6.37 | 3 | 41.17 | 24.10 | 3 |
| | <i>A3G1S1</i> | | | <i>A3G2S1</i> | | | <i>A3G2S2</i> | | | <i>A3G3S1</i> | | |
| Fetuin -S -G | 15.17 | 1.64 | 2 | 8.40 | 0.23 | 2 | 0.00 | 0.00 | 2 | 0.00 | 0.00 | 2 |
| Fetuin -S | 0.72 | 0.37 | 2 | 0.60 | 0.16 | 2 | 0.47 | 0.06 | 2 | 28.09 | 10.44 | 2 |
| Dual column | 1.55 | 1.82 | 3 | 2.73 | 3.64 | 3 | 0.37 | 0.32 | 3 | 37.01 | 24.06 | 3 |
| | <i>A3G3S2</i> | | | <i>A3G3S3</i> | | | | | | | | |
| Fetuin -S -G | 0.67 | 0.95 | 2 | 0.00 | 0.00 | 2 | | | | | | |
| Fetuin -S | 1.16 | 0.59 | 2 | 0.31 | 0.09 | 2 | | | | | | |
| Dual column | 3.72 | 1.49 | 3 | 0.55 | 0.24 | 3 | | | | | | |